Studies on Pharmacological Roles for Inhibitors of Rho Kinases

A Dissertation Submitted to
the Graduate School of Life and Environmental Sciences,
the University of Tsukuba
in Partial Fulfilment of the Requirements
for the Degree of Doctor of Philosophy in Biotechnology
(Doctoral Program in Life Sciences and Bioengineering)

Itsuko BABA

Abbreviations

α-SMA	alpha-smooth muscle actin
CKD	chronic kidney disease
ECM	extracellular matrix
EMT	epithelial mesenchymal transition
HKO	heterozygous knockout
IL-1β	interleukin-1 beta
IL-6	interleukin-6
LPS	lipopolysaccharide
MCP-1	monocyte chemoattractant protein-1
MYPT-1	myosin phosphatase target subunit-1
ROCK	Rho-associated coiled-coil kinase
TGF-β1	transforming growth factor-beta 1
TNFα	tumor necrosis factor alpha
UUO	unilateral ureteral obstruction
WT	wild type

Contents

Chapter I

Preface

Chronic kidney disease (CKD) is the common end-point of renal disease and is defined by a decline in glomerular filtration rate and by structural impairments of the kidney. According to the US Renal Data System 2013 Annual Data Report, 14% of the adult population in the USA had CKD, and the costs for CKD patients older than 65 years were estimated at over 45 billion dollars (1). Patients with CKD require lifelong dialysis, and the only curative treatment for them is kidney transplantation. CKD is a major burden on the healthcare system and is an important predictor of cardiovascular morbidity and mortality. A variety of etiologies such as genetic, autoimmune, infectious, environmental dietary, and medications eventually lead to the same features of CKD. Essentially, almost all CKD progression is characterized by fibrosis in either the glomerulus or the tubulointerstitium (2, 3). Therefore, renal fibrosis is a critical problem for CKD patients.

For studying renal fibrosis, unilateral ureteral obstruction (UUO) is the most widely used model, given that interstitial inflammations occur rapidly and the subsequent histological changes are recognized. These include tubular dilation, tubular atrophy, and fibrosis, which are common alterations observed in several tubulointerstitial diseases (4-7). Many investigators have shown using UUO models that renal interstitial fibrosis is the result of failed wound healing following an initial injury. As shown in

Fig. 1, the pathophysiology of renal fibrosis is classified into four phases: 1) activation and injury; 2) fibrogenic signaling; 3) fibrogenesis; and 4) renal destruction. Interstitial inflammation, tubular activation, and myofibroblast appearance are observed in the kidney in the first phase. Next, the myofibroblasts increase in number, and chemotaxis of fibroblasts and monocytes into the tubulointerstitium begins. In the third phase, extracellular matrix (ECM) accumulates in the injured regions. Finally, ECM accumulation, capillary obliteration, and tubular ischemia appear in the injured kidney, leading to nephron and tubule degeneration (1).

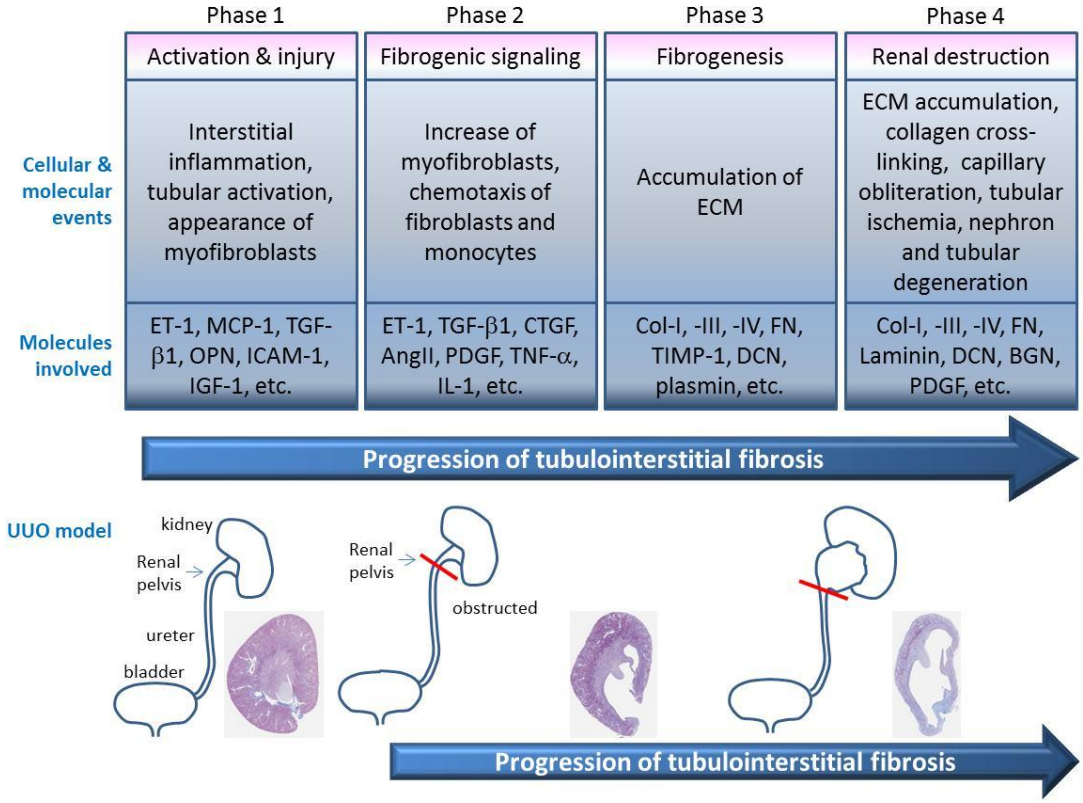

Fig. 1. Progression of renal interstitial fibrosis

The small G-protein, Rho, is known to play a role as a molecular switch in various cellular functions, including cell contraction, adhesion, proliferation, differentiation, and inflammatory response (8-10). Rho-associated coiled-coil kinase (ROCK), a serine/threonine kinase, is a major downstream effector of Rho and is comprised two isoforms, ROCK1 (Rho-kinase β, ROKβ) and ROCK2 (Rho-kinase α, ROKα). In humans, these two kinases have 64% overall identity, 89% identity in the catalytic kinase domain, 55% identity in the coiled-coil region, and 80% identity in the pleckstrin homology (PH) domain (Fig. 2). The expression of ROCK1 is distributed in the kidney, liver, lung, spleen, and testis, whereas ROCK2 is expressed particularly in the heart and brain (11-13). As shown in Fig. 3 and Fig. 4, the Rho/ROCK signaling pathway is involved in several diseases such as cancer, neuronal degradation, cardiovascular diseases, and CKD (14-26).

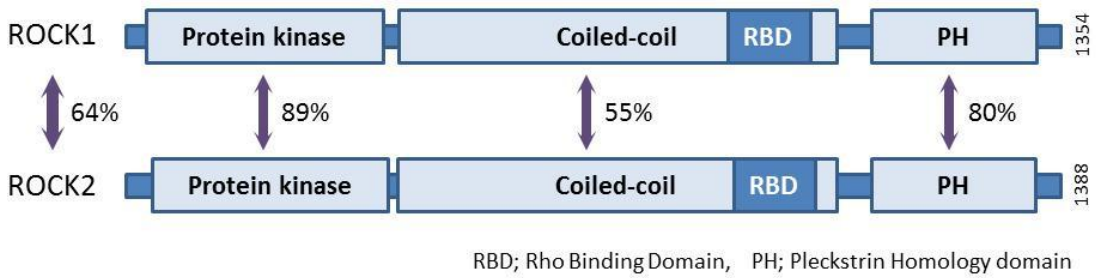

Fig. 2. Functional domains of ROCK1 and ROCK2

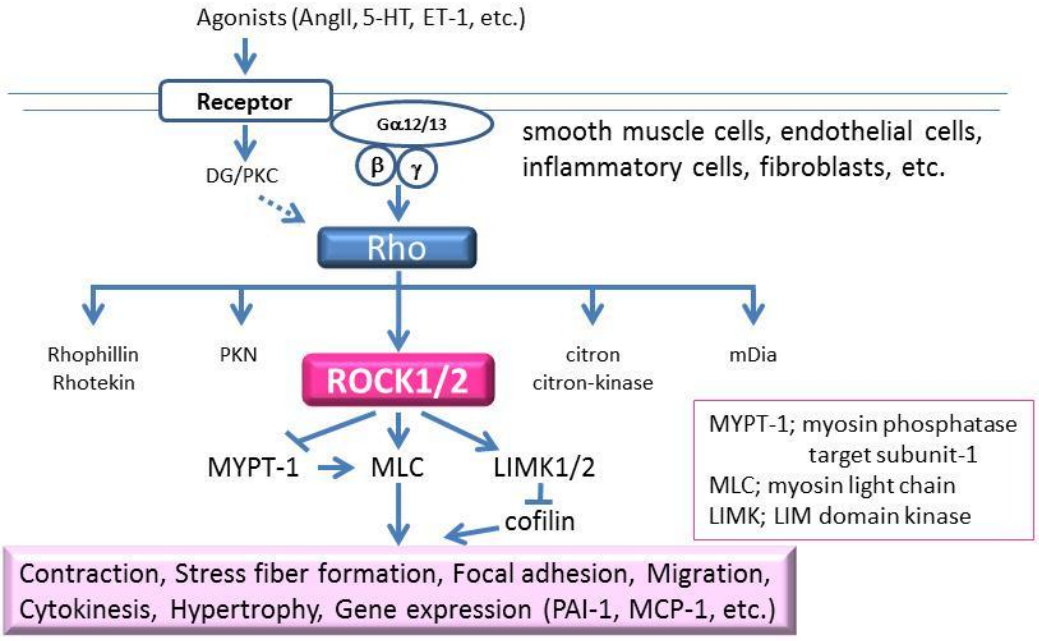

Fig. 3. ROCK and the Rho/ROCK signal pathway.

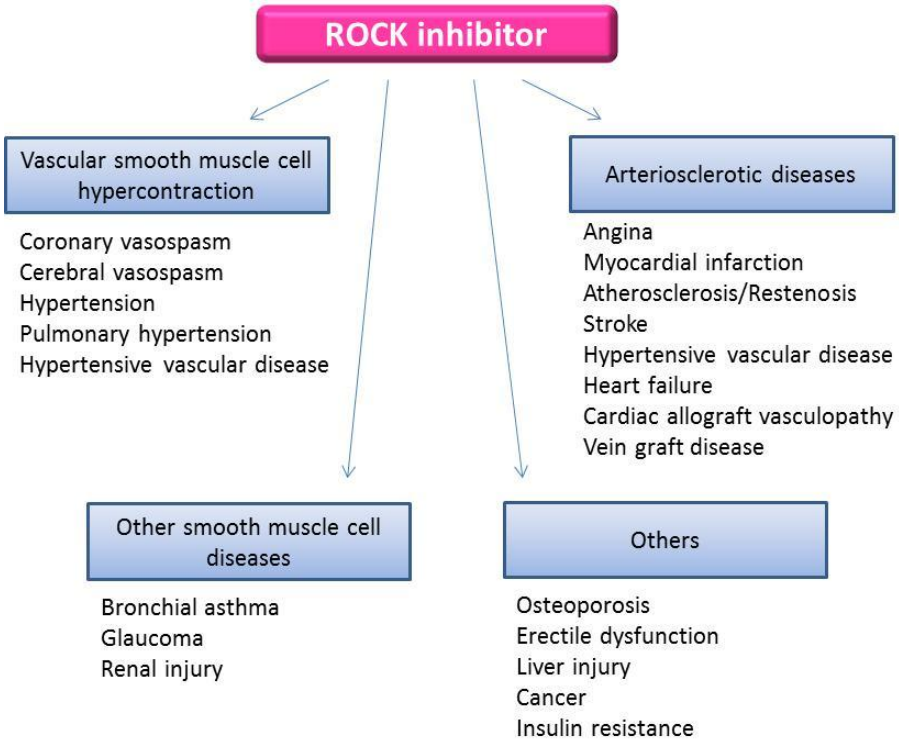

Fig. 4. Therapeutic target for cardiovascular and other diseases

With respect to renal interstitial fibrosis, ROCK inhibition has been investigated using the UUO model. The ROCK inhibitors, fasudil and Y27632, partially attenuate interstitial fibrosis by inhibiting the mRNA expression of collagen, TGF-β1, and α-SMA in the UUO model (27-29). Fasudil and Y27632 specifically inhibit ROCK, although they are non-selective ROCK1 and ROCK2 inhibitors. Fu, *et al*. showed, using ROCK1 knockout (KO) mice, that these mice were not protected against renal fibrosis either early or late after UUO compared with wild-type (WT) mice (30). There were no differences between the ROCK1 KO and WT mice in histological changes or mRNA expression of collagen and α-SMA. However, pharmacological ROCK inhibition effectively suppresses renal interstitial fibrosis in the same study. Thus, given that ROCK1 does not contribute to the suppression of renal interstitial fibrosis by UUO, ROCK2 may play a critical role in renal interstitial fibrosis.

In this study, I investigated the role of ROCK2 on renal interstitial fibrosis induced by UUO, using ROCK2 heterozygous knockout (HKO) mice. I also investigated the underlying mechanisms of ROCK inhibition in renal interstitial fibrosis.

Chapter II

Partial deletion of ROCK2 protein fails to reduce renal fibrosis in mouse unilateral ureteral obstruction model.

Summary

Rho/ROCK signaling is involved in renal fibrotic processes. Non-selective ROCK1/2 inhibitors have been reported to diminish renal interstitial fibrosis in the rodent UUO model. To clarify the role and contribution of ROCK2 in renal fibrosis, I used ROCK2 HKO mice to assess collagen deposition and fibrosis-related gene expression in the kidney of the UUO model. In the ROCK2 HKO mice, the expression level of ROCK2 in the normal kidney was half of that of WT mice. The expression of ROCK1 in both ROCK2 HKO mice and WT mice was equivalent. Furthermore, in the ROCK2 HKO and the WT mice, the hydroxyproline content and the gene expressions of collagen I and TGF-β1 in the obstructed kidneys were augmented after UUO. In contrast, the expression of α-SMA mRNA decreased in the ROCK2 HKO mice compared with that in the WT mice. The ROCK activity of the obstructed kidneys indicated by the phosphorylation of myosin phosphatase target subunit-1 (MYPT-1), which is a non-selective substrate of both ROCK1 and ROCK2, was equivalent among the ROCK2 HKO and WT mice. In conclusion, there was no difference in renal interstitial fibrosis and UUO-induced ROCK activity between the ROCK2 HKO and WT mice,

indicating that a genetic partial disruption of ROCK2 is insufficient in protecting renal fibrosis.

Introduction

Several reports in the cardiovascular field have focused on the relationship between ROCK and tissue fibrosis. In a rat coronary artery occlusion model, the inhibition of ROCK by fasudil, a non-selective ROCK1/2 inhibitor, reduced the expression of inflammatory cytokines such as TGF-β1 and macrophage migration inhibitory factor, and prevented cardiomyocyte hypertrophy and interstitial fibrosis (31). Furthermore, fasudil attenuated the upregulation of profibrotic gene expression such as collagen I and III in the heart after pressure overload in the transverse aortic constriction (TAC) model mice, and ameliorated myocardial remodeling and fibrosis (32). With regard to kidney diseases, fasudil inhibited the activation of ROCK and the TGF-β-Smad pathway, preventing glomerulosclerosis and tubulointerstitial fibrosis in an aldosterone-induced renal injury model (33). In the UUO model, the inhibition of ROCK by Y-27632 or fasudil inhibited the activity of ROCK and gene expression of fibrosis-related factors such as collagen, TGF-β1, and α-SMA, thereby preventing tubulointerstitial fibrosis (27-29). These findings suggest that ROCK plays an important role in the development of tissue fibrosis.

Further investigations using ROCK1 or ROCK2 KO mice have been recently reported. The deletion of ROCK1 suppressed cardiac fibrosis and ventricular remodeling after pressure overload by TAC (34) and protected the development of albuminuria in streptozotocin-induced diabetic kidney

disease model (35). In the cardiac-specific deletion of ROCK2, angiotensin II-induced cardiac hypertrophy and fibrosis were attenuated compared with that of the WT mice (36). These reports as well as previous studies of ROCK inhibitors suggest that both ROCK1 and ROCK2 contribute to cardiac inflammation and fibrosis in the development of heart failure. In contrast, the deletion of ROCK1 did not affect the expression of α-SMA and collagen I and III within the diseased kidney in the UUO model and did not prevent UUO-induced renal fibrosis (30). Thus, the role and contribution of ROCK2 in renal fibrosis remains unestablished. In the present study, I assessed whether ROCK2 is involved in the development of renal fibrosis after UUO in ROCK2 HKO mice.

Materials and methods

All animal experiments were conducted according to the Experimental Animal Care and Use Committee, Mitsubishi Tanabe Pharma Corporation, that was regulated by Management and Ethics of Animal (Law No. 105, 1973, Japan). In addition, this study was performed according to the reliability standards (Article 43 of the Pharmaceutical Affairs Law Enforcement Regulations, Japan).

Animals

Male ROCK2 HKO (37) and WT mice were purchased from Charles River Japan (Charles River Laboratories International, Kanagawa, Japan), were maintained at room temperature on a 12-h light/dark cycle, and were allowed *ad libitum* access to standard laboratory chow (CRF-1, Oriental Yeast, Tokyo, Japan) and tap water. The animals were kept at the department animal care facility of Mitsubishi Tanabe Pharma Corporation in accordance with the relevant protocols.

Unilateral ureteral obstruction model

Mice were anesthetized with sevofrane (Maruishi Pharmaceutical, Osaka, Japan) and subjected to a left flank incision. UUO was performed by a complete ligation of the left ureter at the ureteropelvic junction with a 4-0 silk suture. The sham-operated mice had their ureter exposed without ligation. All mice were used for experiments at 8–10 weeks of age after 1

week of acclimation period. Further, mice were euthanized under anesthesia with sevofrane on days 7 and 14 after operation. Kidneys were then removed and divided into several parts (for RNA, hydroxyproline, and protein sections).

Determination of kidney hydroxyproline content

The collagen content in the kidney was determined by hydroxyproline using a modified method previously described (38, 39). In brief, the kidneys were homogenized in phosphate buffered saline (Gibco, Life Technologies, Carlsbad, CA, USA) (700 ml/100 mg kidney weight), completely hydrolyzed in 6 mol/l HCl (Wako Pure Chemical Industries, Osaka, Japan) at 120°C for 6 h, and filtered through a 0.45-μm Millex-HV filter (Merck Millipore, Hessen, Germany). The samples were dried by vacuum centrifugation using by EZ-2 plus (Genevac, Suffolk, UK) for 16 h. Dried samples were solubilized in distilled water. The samples were oxidized using chloramine T solution [1.4% sodium *p*-toluenesulfonchloramide trihydrate (chloramine T, Wako Pure Chemical Industries) and 10% *n*-propanol (Wako Pure Chemical Industries) in citric acid buffer, which was consisted of 0.26 mol/l citric acid (Sigma-Aldrich), 0.88 mol/l sodium acetate trihydrate (Wako Pure Chemical Industries), 0.85 mol/l sodium hydroxide (Wako Pure Chemical Industries), and 1.2% acetic acid (Kanto Chemical, Tokyo, Japan)]. After incubation at room temperature for 20 min, Ehrlich's solution [1 mol/l 4-dimethylaminobenzaldehyde (Sigma-Aldrich), 18% perchloric acid

(Sigma-Aldrich), and 60% *n*-propanol] was added, and the samples were incubated at 65°C for 40 min. Absorbance was measured at 560 nm (SpectraMax M5e, SoftMax Pro ver. 5.4.1, Molecular Devices, Sunnyvale, CA, USA). The concentration of hydroxyproline was estimated by a standard curve using a pure solution of *l*-hydroxyproline (Wako Pure Chemical Industries). Final results were expressed as hydroxyproline per mg protein. The kidney protein concentration was determined using the BCA protein assay (Pierce, Thermo Scientific, Waltham, MA, USA) with bovine serum albumin as a standard.

Quantitative real-time PCR analyses

Total RNA was extracted from the kidney using TRIzol Reagent (Invitrogen Life Technologies) and purified according to the manufacturer's protocol of RNeasy Mini Kit (74106, QIAGEN, Venlo, Netherlands). Furthermore, the total RNA concentration was determined using NanoDrop 1000 Spectrophotometer (Thermo Scientific). cDNA was synthesized from 1μg of total RNA with SuperScript VILO Master Mix (11755250, Invitrogen, Life Technologies) using the iCycler Thermal Cycler (Bio-Rad, Hercules, CA, USA). Quantitative real-time PCR was performed in 7500 Fast Real-Time PCR System (Applied Biosystems, Life Technologies) using the TaqMan technology. Data was analysed using the standard curve method. The results of each gene were normalized to that of 18SrRNA as an internal control. The following TaqMan Gene Expression Assay reagents (Applied Biosystems, Life Technologies) were used

(TGF-β1, Mm00441724_m1; α-SMA, Mm01546133_m1; collagen 1a2, Mm00483888_m1; 18SrRNA, 4308329).

Western blotting analyses

Kidney tissues were homogenized in a lysis buffer containing 50 mmol/l Tris-HCl pH 8.0 (Nacalai Tesque, Kyoto, Japan), 150 mmol/l NaCl (Wako Pure Chemical Industries), 0.5% sodium deoxycholate (Wako Pure Chemical Industries), 0.1% sodium dodecyl sulfate (Bio-Rad), 1% Triton X-100 (Sigma-Aldrich), 1x protease inhibitors (complete, 11697498001, Roche, Basel, Switzerland), and 1x phosphatase inhibitors (P2850, Sigma-Aldrich). Following centrifugation at 15,000 x g for 20 min at 4°C (CF-15R, Hitachi Koki, Tokyo, Japan), the supernatant was collected as the lysate. The lysates were denatured for 5 min by boiling. Protein concentration was determined using the BCA protein assay (Pierce, Thermo Scientific) with bovine serum albumin as a standard. Equal amounts of lysates were separated on a 4%–15% TGX Precast Gel (Bio-Rad), and transferred to a polyvinyliden difluoride membrane using the Trans-Blot Turbo Transfer System (Bio-Rad). The blots were blocked in Starting Block T20 (PBS) Blocking Buffer (Pierce, Thermo Scientific) at room temperature for 1 h. They were subsequently incubated overnight at 4°C with the primary antibodies [anti-ROCK1 rabbit polyclonal antibody (1:200, H-85, sc-5560, Santa Cruz Biotechnology, Santa Cruz, CA, USA), anti-β-actin mouse monoclonal antibody (1:1000, C4, sc-47778, Santa Cruz Biotechnology), anti-ROCK2 mouse monoclonal antibody (1:5000, 610624,

Transduction Laboratories, BD, Franklin Lakes, NJ, USA), anti-MYPT-1 rabbit polyclonal antibody (1:1000, 2634, Cell Signaling Technology, Danvers, MA, USA), and anti-phospho-MYPT-1 (Thr853) rabbit polyclonal antibody (1:1000, 4563, Cell Signaling Technology)] in Can Get Signal solution (Toyobo, Osaka, Japan). They were then incubated with secondary antibodies [ECL Anti-rabbit IgG, Horseradish Peroxidase-Linked Species-Specific Whole Antibody from donkey (1:5000, NA934, GE healthcare, Buckinghamshire, UK) and ECL Anti-Mouse IgG, Horseradish Peroxidase-Linked Species-Specific Whole Antibody from sheep (1:5000, NA931, GE healthcare)] and developed using enhanced chemiluminescence methods (54-71-00, LumiGLO Reserve Chemiluminescent Substrate Kit, KPL, Gaithersburg, MD, USA). The signal intensities of specific bands were detected using LAS-3000 Luminescent Image Analyzer (Fujifilm, Tokyo, Japan) and analyzed by Multi Gauge program (ver. 3.0, Fujifilm). For quantification, the signal intensities were normalized to β-actin loaded in each well.

Statistical analyses

All data are expressed as means ± standard error mean. Parameters between the sham- and UUO-operated mice or between the WT and ROCK2 HKO mice were compared by Student's t-test. $P < 0.05$ was considered as statistically significant.

Results

Hydroxyproline content in the UUO kidney

To assess renal interstitial fibrosis, I evaluated the collagen accumulation in UUO kidneys. Total kidney collagen deposition was determined by measuring the hydroxyproline content, which significantly increased in the UUO-operated kidney, compared to that of the sham-operated kidney. After the 3 days of UUO, the hydroxyproline content continued to increase (data not shown). At days 7 and 14 after UUO, I compared the WT and HKO mice. Moreover, the hydroxyproline content increased in the UUO-operated kidney of both the WT (2.4- and 4.4-fold at days 7 and 14 after UUO, respectively) and HKO mice (2.6- and 4.1-fold at days 7 and 14 after UUO, respectively, Fig. 5). There was no significant difference.

Expression of collagen I, α-SMA, and TGF-β1 mRNA in the UUO kidneys

I measured the fibrosis-related gene expression to examine the effect of partial ROCK2 deletion. The levels of collagen I, α-SMA, and TGF-β1 mRNA in the UUO-operated kidney of the WT mice markedly increased compared to those in the sham-operated kidney (collagen I, 11.0- and 11.8-fold; α-SMA, 5.1- and 6.9-fold; TGF- β1, 7.9- and 7.9-fold at days 7 and 14 after UUO, respectively). In contrast, the expression level of α-SMA mRNA markedly ameliorated in the HKO mice at day 7 after UUO to 78% of the level noted in the WT mice (Fig. 6B). At day 14 after UUO,

the expression level of α-SMA mRNA in the HKO mice was not statistically significant; however, it was suppressed to 81% of that in the WT mice. Moreover, collagen I and TGF-β1 mRNA expression levels increased in the UUO-operated kidney of HKO mice (collagen I, 9.9- and 10.8-fold; TGF-β1, 6.9- and 7.4-fold at days 7 and 14 after UUO, respectively); their expression levels were almost the same compared with those in the WT mice (Fig. 6A, C).

ROCK activity in the UUO kidneys

To confirm the difference in the ROCK activity between the WT and HKO mice, I measured the phosphorylation of MYPT-1, a target protein of ROCK in the UUO-operated kidney. The phosphorylated MYPT-1 was detected in the UUO-operated kidney of both the WT and HKO mice in a similar manner (Fig. 7), indicating that the ROCK activity did not change the partial ROCK2 deletion. In the normal kidney, ROCK2 protein expression level in the HKO mice was a half of that in the WT mice (Fig. 8). However, the expression level of ROCK1 protein did not change between the WT and HKO mice in the kidney; the expression ratio of ROCK1 and ROCK2 also did not change in the UUO-operated kidney (data not shown).

Discussion

In the present study, I investigated the effects of the partial deletion of ROCK2 protein on fibrosis-related genes and renal interstitial fibrosis in mice UUO model. In the WT mice, the hydroxyproline content and expression of collagen I mRNA in the UUO-operated kidney significantly increased at days 7 and 14 after ureteral occlusion. The fibrotic parameters in the UUO kidney of ROCK2 HKO mice also increased. However, there was no statistical difference between the WT and ROCK2 HKO mice on the increment of these fibrotic parameters in the UUO-operated kidney, suggesting that the partial deletion of ROCK2 protein does not influence renal interstitial fibrosis induced by UUO. It has been reported in normal mice that Y27632, a non-selective ROCK1/2 inhibitor, suppresses the collagen I mRNA expression and collagen deposition in damaged kidney at days 4 and 10 after UUO (27). In rat UUO model, fasudil ameliorated the collagen deposition in damaged kidney at day 16 after UUO (28). These results suggest that the pharmacological inhibition of ROCK can prevent the development of UUO-induced renal interstitial fibrosis. In contrast, other investigators demonstrated that in ROCK1 KO mice, complete ROCK1 deletion did not affect collagen accumulation and collagen I mRNA expression in the UUO kidney at days 5 and 10 after UUO. This suggests that ROCK2, but not ROCK1, is involved in renal interstitial fibrosis in UUO (30). However, in this study, partial ROCK2 deletion indicated a non-significant reduction in renal interstitial fibrosis. Thus, it is

likely that the effect of the pharmacological inhibition of ROCK is inconsistent with that of the deletion of ROCK protein on the development of renal interstitial fibrosis after UUO.

It is evident that TGF-β1 signals and the Rho/ROCK pathway are closely associated with renal interstitial fibrosis by UUO (40). Y27632 is reported to suppress the augmentation of TGF-β1 mRNA expression in UUO mice (27). However, in ROCK1 KO mice, TGF-β1 expression was significantly enhanced in the damaged kidney after UUO compared with the WT mice because the absence of ROCK1 may not be able to suppress TGF-β1 expression to protect renal fibrosis (30). Therefore, ROCK2 was considered to play an important role in TGF-β1 signaling in renal interstitial fibrosis after UUO. In the present study, partial ROCK2 deletion did not suppress TGF-β1 and ROCK1 mRNA expression, and ROCK activity remained unaffected in the UUO-operated kidney. These results suggest that the response to partial ROCK2 deletion is distinct from that to pharmacological ROCK inhibition.

In renal interstitial fibrosis, the transformation to myofibroblasts, which are considered to be the dominant collagen producing cells, is a crucial step toward collagen synthesis and deposition. In kidney fibrosis, the resident fibroblast, epithelial, endothelial, and bone marrow-derived cells can acquire the myofibroblast phenotype and express the characteristic proteins, such as α-SMA. Further, the ROCK signaling pathway is reported to play an important role in cell transformation to activated myofibroblasts (41, 42). In the present study, the level of α-SMA expression markedly decreased in

the UUO kidney of ROCK2 HKO mice compared with that of the WT mice. In ROCK1 KO mice, the augmentation of α-SMA mRNA and protein caused by UUO were not decreased (30). Thus, it is likely that ROCK2 may be implicated in UUO-induced transformation via any signal cascade independent of TGF-β1. In addition, I found in mice UUO model that the effect of ROCK2 HKO is inconsistent with that of the pharmacological inhibition of ROCK. With respect to the inconsistence, ROCK inhibitors are considered to be poor in isoform selectivity and other target specificity. Y-27632 and fasudil equivalently inhibit both ROCK1 and ROCK2 activity; fasudil also inhibits PKN, PKC, myosin light chain kinase, and MEK1. It must be considered that the partial deletion of ROCK2 may be insufficient in suppressing UUO-induced fibrotic responses. Moreover, it is possible that the results depend on experimental procedures and pathophysiological conditions in the UUO model. In order to solve these problems, further studies are required using a kidney-specific ROCK1 or ROCK2 deletion and using more specific inhibitors for ROCK1 or ROCK2. In conclusion, using ROCK2 HKO mice, I demonstrated that the partial deletion of ROCK2 as well as ROCK1 inhibition is insufficient in effectively preventing renal interstitial fibrosis.

Figures

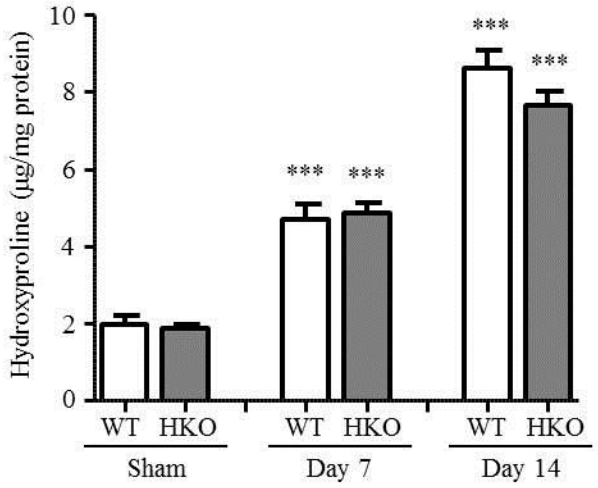

Fig. 5. The hydroxyproline content in the kidney of WT and HKO mice at days 7 and 14 after UUO

The hydroxyproline content in the kidney of the UUO operated mice was compared with that of the sham-operated mice at days 7 and 14 after UUO. The symbols are WT mice (open bar) and HKO mice (solid bar). Results are expressed as mean ± SEM (n = 5–10). *** $P < 0.001$ compared to the sham group.

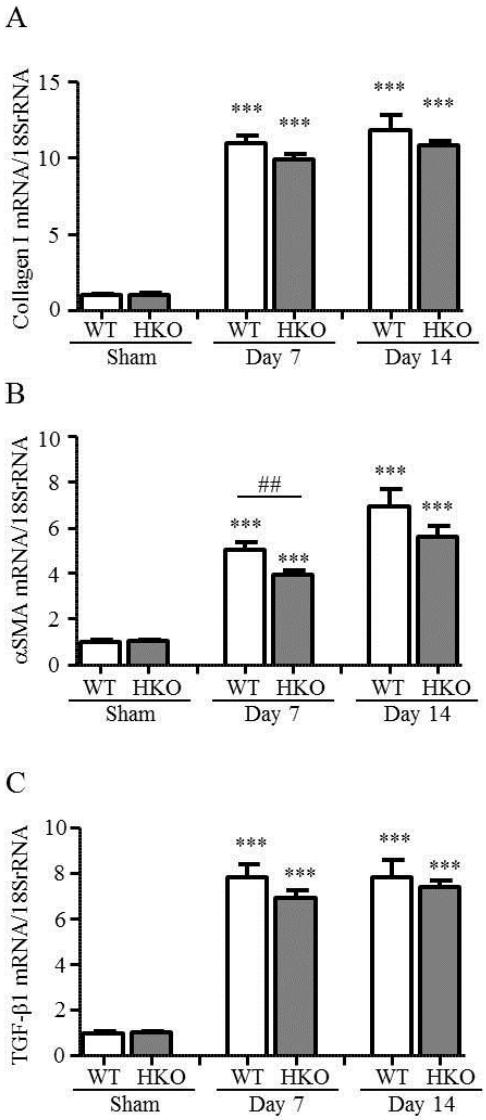

Fig. 6. Collagen I, α-SMA, and TGF-β1 mRNA expression in the kidney of WT and HKO mice at days 7 and 14 after UUO

Collagen I (A), α-SMA (B), and TGF-β1(C) mRNA expression in the UUO-operated mice were compared with that in the sham-operated mice at days 7 and 14 after UUO. The symbols are WT mice (open bar) and HKO mice (solid bar). Results are expressed as mean ± SEM (n = 5–10). ****P* < 0.001 compared to sham group and ##*P* < 0.01 compared to WT mice at the same time point.

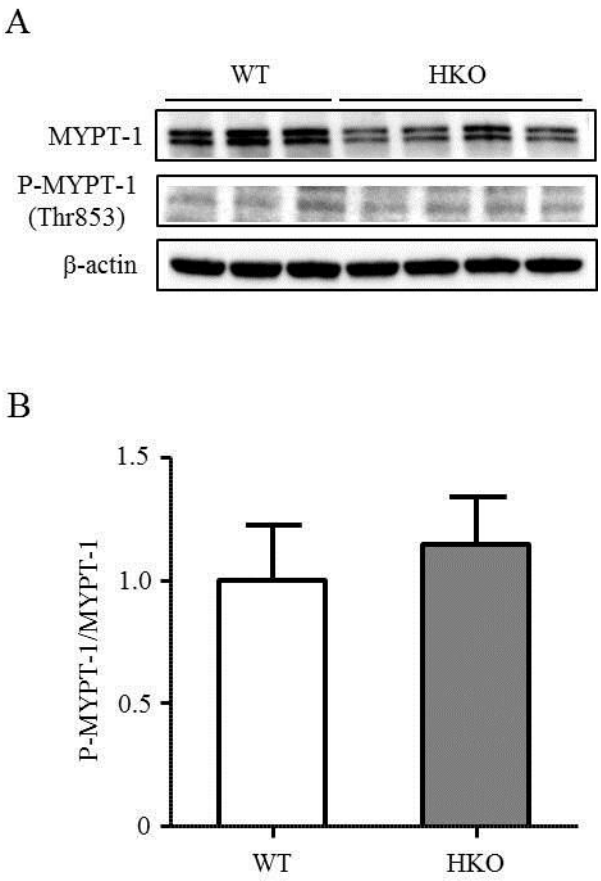

Fig. 7. The ROCK activity of WT and HKO mice in the kidney

(A) Representative western blotting photographs demonstrate the levels of MYPT-1 (upper panel) and phospho-MYPT-1 (middle panel) proteins in the kidney of WT and HKO mice at day 7 after UUO. The same blot was detected with β-actin (lower panel) to confirm equal loading. (B) Quantitative analysis shows the relative abundance of the phospho-MYPT-1/MYPT-1 ratio after normalization with β-actin. Results are expressed as mean ± SEM (n = 3–5). The symbols are WT mice (open bar) and HKO mice (solid bar).

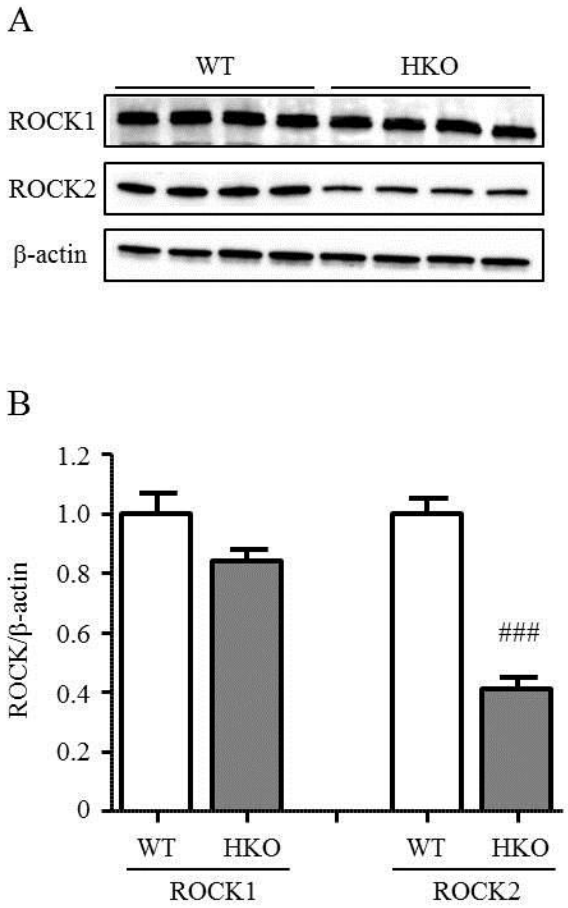

Fig. 8. ROCK1 and ROCK2 proteins expression of WT and HKO mice in the normal kidney

(A) Representative western blotting photographs demonstrate the levels of ROCK1 (upper panel) and ROCK2 (middle panel) proteins in the normal kidney of WT and HKO mice. The same blot was detected with β-actin (lower panel) to confirm equal loading. (B) Quantitative analysis shows the relative abundance of the ROCK1 or ROCK2 protein after normalization with β-actin. Results are expressed as mean ± SEM (n = 7). The symbols are WT mice (open bar) and HKO mice (solid bar). ###$P < 0.001$ compared to WT mice.

Chapter III

The inhibitory effects of fasudil on renal interstitial fibrosis induced by unilateral ureteral obstruction

Summary

Several studies have reported that ROCK inhibitors attenuate renal fibrosis. However, the mechanism of this process is still incompletely understood. I assessed the inhibitory effect of fasudil, a ROCK inhibitor, *in vivo* and *in vitro* to elucidate the mechanisms underlying renal interstitial fibrosis. In mice with UUO, the collagen accumulation, fibrosis-related gene expression, and hydroxyproline content in the kidney increased 3, 7, and 14 days after UUO. Fasudil attenuated the histological changes and the production of collagen and ECM in the UUO kidney. The expression of α-SMA, TGF-β-Smad signaling pathway, and macrophage infiltration were suppressed by fasudil in the kidneys of the UUO mice. I also evaluated the role of intrinsic renal cells and infiltrated macrophages using NRK-52E, NRK-49F, and RAW264.7 cells. The mRNA and protein expression of collagen I and α-SMA increased in NRK-52E and NRK-49F cells stimulated by TGF-β1. Hydroxyfasudil, a bioactive metabolite of fasudil, attenuated the increase in α-SMA mRNA and protein expression levels in both cell types. However, the reduction in collagen I mRNA levels was observed in NRK-49F cells alone. Hydroxyfasudil decreased MCP-1 mRNA expression induced by TGF-β1 in NRK-52E but not in NRK-49F

cells. In RAW264.7 cells, MCP-1, IL-1β, IL-6, and TNFα mRNA expression, significantly elevated by lipopolysaccharide (LPS) stimulation, was not suppressed by hydroxyfasudil. These data suggested that the inhibition of ROCK suppressed renal interstitial fibrosis via TGF-β-Smad signaling pathway and decreased the infiltration of macrophages to the injured kidney. However, the cytokine/chemokine expression in macrophages was unaffected. It is likely that ROCK contributes to the activation of renal intrinsic cells and migration of extra-renal cells in the progression of renal interstitial fibrosis.

Introduction

Fasudil and Y27632, the non-selective ROCK1/2 inhibitor, have been used to evaluate the role of ROCK in several animal disease models. In the rat heart ischemia-reperfusion (IR) model, fasudil reduces the infarct size by attenuating endoplasmic reticulum stress and modulating SERCA activity (43). Similarly, in rat kidney IR model, fasudil suppresses the renal injury and improves kidney function (44). Furthermore, fasudil shows the renoprotective effects such as improving albuminuria and mesangial matrix expansion. It also suppresses renal injury by downregulation of hypoxia-inducible factor 1α in diabetic nephropathy model (45). Some *in vitro* studies, using mesangial, tubular epithelial, or kidney fibroblast cells (46-48), have reported that Y27632 inhibits cell hypertrophy, expression of α-SMA, and collagen expression induced by aldosterone or TGF-β1. These reports have suggested that ROCK inhibitors use a variety of functional mechanisms and are effective in a wide range of diseases.

Renal tubulointerstitial fibrosis is a common pathway in progressive renal diseases. The UUO model is widely used in the studies of progressive interstitial fibrosis that is independent of hypertension or systemic immune disease. After UUO, the obstructed kidney exhibits a substantial macrophage influx into the interstitium and develops tubulointerstitial fibrosis. Fasudil and Y27632 have been reported to prevent tubulointerstitial fibrosis in the UUO model by inhibiting the expression of collagen, TGF-β1, and α-SMA mRNAs (27-29). However, the details of

the mechanism are still incompletely understood. In this study, I investigated the effect of a ROCK inhibitor on renal interstitial fibrosis, renal intrinsic cells, and the cells infiltrating the kidney.

Materials and methods

All animal experiments were conducted according to the Experimental Animal Care and Use Committee, Mitsubishi Tanabe Pharma Corporation, that was regulated by Management and Ethics of Animal (Law No. 105, 1973, Japan). In addition, this study was performed according to the reliability standards (Article 43 of the Pharmaceutical Affairs Law Enforcement Regulations, Japan).

Animals

Male C57BL/6J mice were purchased from Charles River Japan; they were maintained at room temperature on a 12-h light/dark cycle and allowed *ad libitum* access to standard laboratory chow (CRF-1) and tap water. The animals were kept at the departmental animal care facility of Mitsubishi Tanabe Pharma Corporation in accordance with the relevant protocols.

Unilateral ureteral obstruction model

Mice were anesthetized with sevofrane and subjected to a left flank incision. UUO was performed by a complete ligation of the left ureter at the ureteropelvic junction with a 4-0 silk suture. The sham-operated mice had their ureter exposed without ligation. All mice were used in the experiments at 9 weeks of age after 1 week of the acclimation period.

UUO-operated mice were randomly divided into the following groups: sham, UUO-control, and UUO-fasudil (1 g/l, Mitsubishi Tanabe Pharma, Osaka, Japan). Fasudil was given in drinking water 2 days before UUO operation until the day of sacrifice. The mice were euthanized under anesthesia with sevofrane on days 3, 7, and 14 after operation. Kidneys were then removed and divided into several parts (for RNA, hydroxyproline, immunohistochemistry assays, and protein sections).

Cell culture

The rat kidney tubular epithelial cell line (NRK-52E), fibroblast cell line (NRK-49F), and the mouse macrophage cell line (RAW264.7), obtained from the American Type Culture Collection (ATCC, Manassas, VA, USA), were cultured in low glucose (5 mmol/l) Dulbecco's modified Eagle's medium (D6046, Sigma-Aldrich) supplemented with 10% fetal bovine serum (S1820, Biowest, Nuaille, France) at 37°C under 5% CO_2 atmosphere. For experimental treatments, serum was reduced to 1% for 20 h and recombinant human TGF-β1 (10 ng/ml, 100-21C, Peprotech, Rocky Hill, NJ, USA) or LPS (500 ng/ml, L4391, Sigma-Aldrich) was added for 24 h. To investigate the role of ROCK under these conditions, 10 or 30 μmol/l of hydroxyfasudil (Mitsubishi Tanabe Pharma), a bioactive metabolite of fasudil, was added to the cells 1 h before TGF-β1 or LPS stimulation.

Histology and Immunohistochemistry

The kidneys were removed and immediately fixed in 10% formaldehyde neutral buffer solution (Nacalai Tesque). The formalin-fixed kidneys were embedded in paraffin. Paraffin sections were stained with hematoxylin (115938, Merck, Darmstadt, Germany) and eosin (115935, Merck), and Sirius Red (365548, Sigma-Aldrich)/Fast Green (069-00032, Wako Pure Chemical Industries, Osaka, Japan). Immunohistochemistry was performed as described previously (49). Briefly, kidney paraffin sections were deparaffinized. Sections were pretreated with 3% hydrogen peroxide. The sections were incubated overnight at 4°C with anti-α-SMA mouse monoclonal antibody (1:500, A2547, Sigma-Aldrich) or anti-F4/80 rat monoclonal antibody (1:100, MCA497G, AbD Serotec, Kidlington, UK) followed by the incubation with HRP-conjugated anti-mouse IgG secondary antibody (414321, Histofine Mouse Stain kit, Nichirei Biosciences, Tokyo, Japan) and HRP-conjugated anti-rat IgG secondary antibody (414311, Histofine Simple Stain Mouse MAX PO Rat, Nichirei Biosciences), respectively. The sections were colorized with 3,3′-diaminobenzidine (Nacalai Tesque) and counterstained with hematoxylin (30002, Muto Pure Chemicals, Tokyo, Japan). The sections were photographed with a DP73 digital camera system (Olympus, Tokyo, Japan) equipped with cellSens software (Olympus) and a BX51 microscope (Olympus). For image analysis, whole-slide digital images of the sections were obtained with Aperio Scan Scope XT (Leica Microsystems, Wetzlar, Germany). Sirius Red-, α-SMA-, and F4/80-positive areas were determined

using Image-Pro Plus software (Media Cybernetics, Bethesda, MD, USA) as described previously (49).

Determination of kidney hydroxyproline content

The collagen content in the kidney was determined using hydroxyproline assay (modified as previously described) (38, 39). In brief, the kidneys were homogenized in phosphate-buffered saline (700 ml/100 mg kidney weight), completely hydrolyzed in 6 mol/l HCl at 120°C for 6 h, and filtered through a 0.45-μm Millex-HV filter. The samples were dried by vacuum centrifugation using EZ-2 plus for 16 h. Dried samples were solubilized in distilled water. The samples were oxidized using chloramine T solution (1.4% sodium *p*-toluenesulfonchloramide trihydrate and 10% *n*-propanol in citric acid buffer, which was consisted of 0.26 mol/l citric acid, 0.88 mol/l sodium acetate trihydrate, 0.85 mol/l sodium hydroxide, and 1.2% acetic acid). After incubation at room temperature for 20 min, Ehrlich's solution (1 mol/l 4-dimethylaminobenzaldehyde, 18% perchloric acid, and 60% *n*-propanol) was added, and the samples were incubated at 65°C for 40 min. Absorbance was measured at 560 nm. The concentration of hydroxyproline was estimated from a standard curve prepared using a pure solution of *l*-hydroxyproline. Final results were expressed as hydroxyproline per mg of protein. The kidney protein concentration was determined using the BCA protein assay with bovine serum albumin as a standard.

Quantitative real-time PCR analyses

Total RNA was extracted from the kidney and cultured cells using TRIzol Reagent and purified according to the RNeasy Mini Kit manufacturer's protocol. The total RNA concentration was determined using NanoDrop 1000 Spectrophotometer. cDNA was synthesized from 1μg of total RNA with SuperScript VILO Master Mix using the iCycler Thermal Cycler. Quantitative real-time PCR was performed in 7500 Fast Real-Time PCR System using the TaqMan technology. Data was analysed using the standard curve method. The results for each gene were normalized to 18SrRNA (an internal control). The following TaqMan Gene Expression Assay reagents were used: ROCK1 (Mm00485745_m1), ROCK2 (Mm00485761_m1), TGF-β1 (Mm00441724_m1), α-SMA (Mm01546133_m1, Rn01759928_g1), collagen 1a2 (Mm00483888_m1, Rn01526721_m1), collagen 3a1 (Mm01254477_m1), fibronectin (Mm01256744_m1), MCP-1 (Mm00441242_m1, Rn00580555_m1), F4/80 (Mm00802529_m1), IL-1β (Mm00434228_m1), TNFα (Mm00443258_m1), IL-6 (Mm00446190_m1), and 18SrRNA (4308329).

Western blotting analyses

Kidney tissues and cultured cells were homogenized in a lysis buffer containing 50 mmol/l Tris-HCl pH 8.0, 150 mmol/l NaCl, 0.5% sodium deoxycholate, 0.1% sodium dodecyl sulfate, 1% Triton X-100, 1x protease inhibitors, and 1x phosphatase inhibitors. Following centrifugation at 15,000 x g for 20 min at 4°C, the supernatant was collected as the lysate.

The lysates were denatured for 5 min by boiling. Protein concentration was determined using the BCA protein assay with bovine serum albumin as a standard. Equal amounts of lysates were separated on a 4%–15% TGX Precast Gel, and transferred to a polyvinylidene difluoride membrane using the Trans-Blot Turbo Transfer System. The blots were blocked in Starting Block T20 (PBS) Blocking Buffer at room temperature for 1 h. They were subsequently incubated overnight at 4°C with the primary antibodies [anti-phospho-MYPT-1 (Thr850) rabbit polyclonal antibody (1:1000, 36-003, Merck Millipore), anti-GAPDH mouse monoclonal antibody (1:500, MAB374, Merck Millipore), anti-collagen type I rabbit polyclonal antibody (1:2000, ABT123, Merck Millipore), anti-phospho-Smad3 (Ser423 + Ser425) rabbit polyclonal antibody (1:2000, ab51451, Abcam, Cambridgeshire, UK), anti-α-SMA rabbit polyclonal antibody (1:500, 14395-1-AP, Proteintech, Chicago, IL, USA)] in Can Get Signal solution. They were then incubated with secondary antibodies [ECL Anti-rabbit IgG, Horseradish Peroxidase-Linked Species-Specific Whole Antibody from donkey (1:5000) and ECL Anti-Mouse IgG, Horseradish Peroxidase-Linked Species-Specific Whole Antibody from sheep (1:5000)] and developed using enhanced chemiluminescence methods. The signal intensities of specific bands were detected using LAS-3000 Luminescent Image Analyzer and analyzed by Multi Gauge program (ver. 3.0). For quantification, the signal intensities were normalized to GAPDH loaded in each well.

Statistical analyses

All data are expressed as means ± standard error. The comparisons between the sham- and UUO-operated control mice, the control and fasudil-treated mice, the non-stimulated cells and stimulated cells, and between the stimulated cells and hydroxyfasudil-treated cells were conducted using Student's t-test. $P < 0.05$ was considered statistically significant.

Results

Effect of fasudil on renal histological changes

The kidneys of the UUO mice progressively developed renal parenchymal thinning accompanied by severe tubulointerstitial damage including tubular atrophy/dilation, tubular regeneration, and interstitial infiltration (Fig. 9) as reported previously (4, 5). Fasudil administration had a little effect on these changes.

Effect of fasudil on the interstitial fibrosis

To determine the effect of fasudil on interstitial fibrosis in the kidneys of the UUO mice, we stained the collagen in the interstitium with Sirius Red and measured the hydroxyproline content and extracellular matrix mRNA expression. In the obstructed kidney, the Sirius Red-positive areas in the renal interstitium increased progressively in comparison with those in the sham-operated kidney during the 14-day period (2.7-, 3.5-, and 6.0-fold increase at days 3, 7, and 14 after UUO, respectively, Fig. 10A and 10B). The content of hydroxyproline was also augmented (1.9-, 3.2-, and 6.6-fold at days 3, 7, and 14 after UUO, respectively, Fig. 10C). Furthermore, the expression levels of mRNAs for collagen I, III, and fibronectin were higher in the kidneys of the UUO mice than in the sham group (collagen I, 7.4-, 14.3-, and 21.3-fold; collagen III, 11.9-, 20.9-, and 35.2-fold; fibronectin, 6.6-, 17.4-, and 31.0-fold at days 3, 7, and 14 after UUO, respectively, Fig. 11A–11C). On day 14 after UUO, administration of fasudil significantly

suppressed these augmented levels. On day 7 after UUO, the Sirius Red-positive areas and fibronectin mRNA expression did not significantly decrease. However, the expression of collagen I and III mRNA and hydroxyproline content in the injured kidney were markedly suppressed by fasudil administration. These results suggest that fasudil ameliorates the interstitial fibrosis.

Effect of fasudil on the α-SMA expression

I next examined the effect of fasudil on interstitial myofibroblasts (characterized by the expression of α-SMA). Immunohistochemical staining showed larger numbers of α-SMA-positive cells in the interstitium of the UUO mice than in the sham-operated mice (12.3-, 16.4-, and 7.2-fold increase at days 3, 7, and 14 after UUO, respectively, Fig. 12A and 12B). Similarly, the expression of α-SMA mRNA increased in the UUO mice (5.9-, 5.6-, and 10.5-fold at days 3, 7, and 14 after UUO, respectively, Fig. 12C). Both immunohistochemical staining and mRNA expression analysis (showing reduction of 65% and 28%, respectively) on day 7 after UUO demonstrated that fasudil administration markedly inhibited the increase in α-SMA expression in the interstitium. Furthermore, the mRNA expression was significantly suppressed on day 14 after UUO (reduced by 17%). These results indicate that fasudil administration inhibits the transformation of renal cells or extra-renal cells to myofibroblasts or the proliferation of myofibroblasts.

Effect of fasudil on the macrophage infiltration

ROCK inhibitors have the ability to suppress the cell migration. I examined the F4/80-positive cells and F4/80 mRNA expression to assess the effect of fasudil on the macrophage infiltration to the kidney. The immunohistochemical staining detected the F4/80-positive cells in the interstitium of the injured kidney; their number in UUO mice progressively increased in comparison with the sham group (3.0-, 22.7-, and 30.2-fold at days 3, 7, and 14 after UUO, respectively, Fig. 13A and 13B). Fasudil administration clearly inhibited the macrophage infiltration into the injured kidney (the numbers reduced by 55% and 28% at days 7 and 14 after UUO, respectively). Similarly, the F4/80 mRNA expression was augmented (2.0-, 5.5-, and 10.0-fold at days 3, 7, and 14 after UUO, respectively, Fig. 13C); this increase was significantly inhibited by administration of fasudil on day 14 after UUO. However, the augmented expression of MCP-1 mRNA was not affected by fasudil (Fig. 13D). These results suggest that fasudil inhibits the migration of macrophages to the injured kidney but does not affect the MCP-1 expression.

Effect of fasudil on the ROCK activity

To confirm the effect of fasudil on the ROCK activity, I measured the phosphorylation of MYPT-1 in the kidney. The level of phosphorylation increased in the obstructed kidney in comparison with sham group (1.4-, 1.4-, and 1.7-fold at days 3, 7, and 14 after UUO, respectively, Fig. 14A). Fasudil treatment did not have a statistically significant effect on the

phosphorylation levels; however, ROCK activity was suppressed to the basal level. The expressions of ROCK1 and ROCK2 mRNA increased in UUO mice, but fasudil did not affect the expressions of these mRNA (Fig. 14B and 14C).

Effect of fasudil on the TGF-β-Smad signaling pathway

It is known that TGF-β-Smad signaling pathway is activated in the kidney of the UUO mice. To examine the effect of fasudil on this pathway, I measured the expression of TGF-β1 mRNA and the level of phosphorylated Smad3. The expression of TGF-β1 mRNA increased in UUO kidneys (3.0-, 6.0-, and 7.2-fold at days 3, 7, and 14 after UUO, respectively, Fig. 15A) in comparison with that in the sham-group kidneys. Fasudil administration significantly suppressed this increase in the obstructed kidney (by 18%) on day 14. In the kidneys of the UUO mice, the level of phosphorylated Smad3 progressively increased in comparison with that in the sham-operated kidneys (3.8-, 5.3-, and 13.1-fold at days 3, 7, and 14 after UUO, respectively, Fig. 15B). This increase was markedly reduced by fasudil (by 29% on day 3 and 37% on day 7 after UUO). These results demonstrated that fasudil blocked the TGF-β-Smad signaling pathway involved in the interstitial fibrosis.

Effect of hydroxyfasudil on the NRK-52E and NRK-49F cells

These results from animal experiments indicated that fasudil attenuated the renal interstitial fibrosis and migration of macrophages to the kidney

interstitium. Using NRK-52E and NRK-49F cells, I also determined the effect of fasudil on the intrinsic renal cells. In the kidney of UUO mice, TGF-β1 is recognized as a vital mediator in renal fibrosis. In NRK-52E and NRK-49F cells, TGF-β1 induced the expressions of α-SMA and collagen I mRNA and their proteins (Fig. 16A and 16B). Hydroxyfasudil, a bioactive metabolite of fasudil, particularly decreased α-SMA mRNA expression induced by TGF-β1 in both cell types. Furthermore, in NRK-49F cells, α-SMA protein production was markedly reduced by 30 μmol/l hydroxyfasudil treatment. However, in NRK-52E cells, the augmentation of α-SMA protein production did not found in this condition. In NRK-49F cells, the increased expression of collagen I mRNA was significantly attenuated by 30 μmol/l hydroxyfasudil treatment; however, the protein production was unaffected. In contrast, in NRK-52E cells, hydroxyfasudil did not affect the levels of collagen I mRNA or its protein. In the kidneys of UUO mice, MCP-1 mRNA expression level increased in comparison with the level in the sham-operated kidneys. These increased levels were unaffected by fasudil (Fig. 13D). The expression of MCP-1 mRNA was stimulated by TGF-β1 in both NRK-52E and NRK-49F cells. Pretreatment with hydroxyfasudil clearly suppressed the induction of MCP-1 mRNA expression in NRK-52E cells but had no effect in NRK-49F cells (Fig. 16C).

Effect of hydroxyfasudil on RAW264.7 cell

The migration of macrophages to the kidney interstitium has been

observed in the UUO model. At an early stage of the UUO, M1 macrophages, the classically activated macrophages, infiltrate the kidney and are involved in the inflammation and phagocytosis (50). I used RAW264.7 cells, stimulated by LPS, as M1 subtype cells. In these activated RAW264.7 cells, the expression of MCP-1, IL-1β, IL-6, and TNFα mRNAs was dramatically augmented (Fig. 17A-17D). Hydroxyfasudil did not affect the expression levels of these mRNA.

Discussion

The UUO model is useful for examination of the mechanisms of tubulointerstitial fibrosis *in vivo*. The interstitial inflammation occurs rapidly (2–3 days) and the subsequent histological changes such as tubular dilation, tubular atrophy, and fibrosis are observed soon after (~7 days). These common alterations are found in several tubulointerstitial diseases (2-7, 51). A study of the ROCK1 KO mice (30) has reported no inhibition of the interstitial fibrosis, although pharmacological inhibitors, fasudil and Y27632, inhibit the fibrosis in UUO model (27-29). To clarify the mechanisms of suppression of the interstitial fibrosis, I investigated the inhibition of ROCK using the pharmacological ROCK inhibitor, fasudil.

I demonstrated that fasudil reduced the renal interstitial fibrosis and attenuated the histological changes in the UUO mice. The results of immunohistochemical staining and mRNA expression analysis showed that fasudil markedly suppressed α-SMA expression in the injured kidney. In the process of the kidney fibrosis, the number of myofibroblasts producing extracellular matrix proteins increases in the tubular interstitium. These cells express a distinctive protein, α-SMA. Until recently, tubular epithelial cells have been considered the main source of the interstitial myofibroblasts. However, many studies have reported that the transformation to myofibroblasts occurs in various cells such as epithelial cells, endothelial cells, bone marrow-derived cells, resident fibroblasts, and pericytes (52-56). In this study, I used a tubular epithelial cell line,

NRK-52E, and a fibroblast cell line, NRK-49F, to examine the transformation to myofibroblasts and analyze the fibrosis-related gene expressions. In NRK-49F cells, hydroxyfasudil attenuated the α-SMA mRNA and protein expression stimulated by TGF-β1. I observed that the upregulated collagen I mRNA expression was suppressed by high dose-hydroxyfasudil in NRK-49F cells only. These results suggest that fasudil inhibits TGF-β1-induced transformation and collagen synthesis in renal fibroblast cells. In NRK-52E cells, hydroxyfasudil suppressed the α-SMA mRNA expression induced by TGF-β1, but it did not increase the α-SMA protein levels. It is possible that the basal expression level of α-SMA is higher than that of other cells under those conditions. Both *in vitro* and *in vivo* studies have reported that not only TGF-β1 but also other stimuli such as angiotensin II, aldosterone, and high glucose induce collagen production in tubular epithelial cells or fibroblast cells, and ROCK inhibitors reduce the collagen production (47, 57, 58). It is possible that other stimuli, but not TGF-β1, induce the fibrotic responses in NRK-52E cells. Thus the inhibition of ROCK suppresses several fibrotic responses in tubular epithelial cells and renal fibroblast cells *in vivo*.

It has been reported that damaged tubular cells, interstitial myofibroblasts, and macrophages produce cytokines, chemokines, and growth factors in the UUO kidneys, triggering the accumulation of interstitial macrophages (59-61). In this study, fasudil inhibited the infiltration of macrophages into the injured kidney. However, the expression of MCP-1 mRNA was not affected by fasudil administration. In NRK-49F cells, hydroxyfasudil did

not reduce the TGF-β1-enhanced MCP-1 mRNA expression. In NRK-52E cells, hydroxyfasudil markedly inhibited the increase in MCP-1 mRNA expression stimulated by TGF-β1. Myofibroblasts in the injured kidney are consisted of several different cell types (52-56). It is reported that myofibroblasts derived from epithelial cells is small population. In this study, hydroxyfasudil inhibited the MCP-1 mRNA expression in the epithelial, NRK-52E cells. Thus it is likely that fasudil is able to suppress the MCP-1 production in myofibroblasts that are derived from epithelial cells. However, these populations are small in comparison with that of other myofibroblast groups; therefore, fasudil may not be able to suppress the MCP-1 expression in the overall myofibroblast cell population in the injured kidney. Several investigators have also reported that the renal interstitial fibrosis can be reduced without inhibition of MCP-1 mRNA expression in UUO mice: however, the mechanism has not been clarified (62-64). Thus the precise relationship between MCP-1 and ROCK in the renal interstitial fibrosis process remains unclear.

Macrophages are categorized into two functional phenotypes: classically activated M1 and alternatively activated M2 (65, 66). In the first stage of UUO kidney injury, almost all the infiltrated macrophages show the M1 phenotype (50). To examine the relationship between macrophages and ROCK in the renal interstitial fibrosis, I assessed LPS-induced inflammatory response in RAW264.7 cells. LPS stimulation elevated the expression of MCP-1, IL-1β, IL-6, TNFα, and iNOS mRNAs, but it was difficult to detect the expression of collagen and TGF-β1 mRNA (data not

shown). These gene expression patterns are characteristic for the phenotype of M1 macrophages. Fasudil treatment did not affect the expression of the genes induced by LPS in RAW264.7 cells. These new results suggest that ROCK may contribute to the infiltration of monocytes/macrophages into the interstitium of the injured kidney rather than affect the inflammatory cytokine/chemokine expression.

Taken together, these data suggest that the inhibition of ROCK suppresses the renal interstitial fibrosis via TGF-β-Smad signaling pathway and the infiltration of macrophages to the injured kidney. It is likely that ROCK contributes to the activation of the renal intrinsic cells and migration of the extra-renal cells in the progression of renal interstitial fibrosis.

Figures

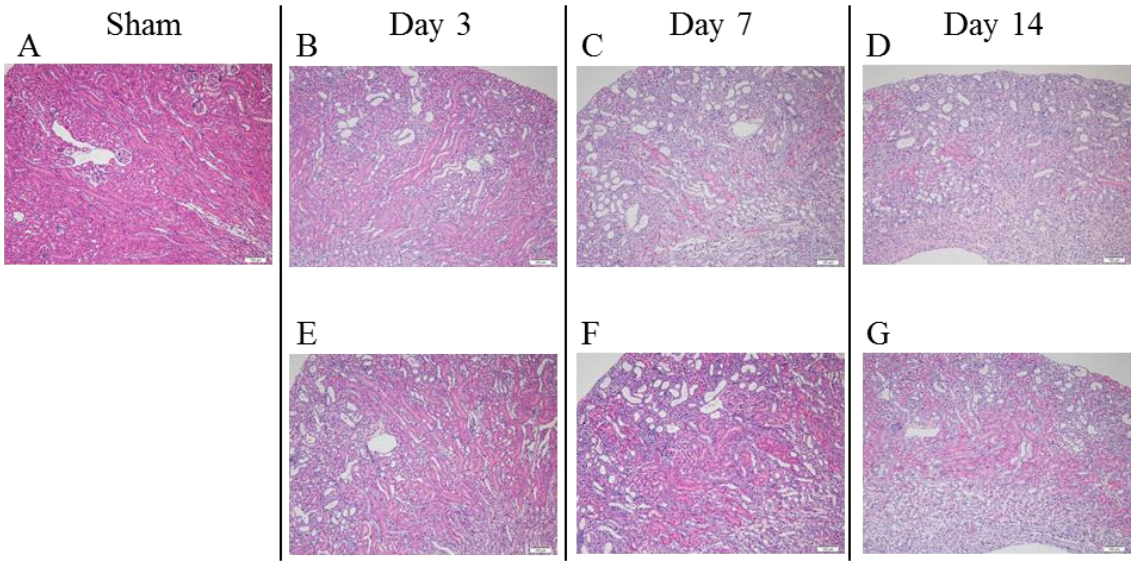

Fig. 9. Histological changes in the kidney

The HE-stained sections of the sham- and UUO-operated kidneys. Sham (A), UUO-control (B-D), UUO-fasudil (E-G) at days 3, 7, and 14 after UUO, respectively (original magnification x10, scale bars: 100 μm).

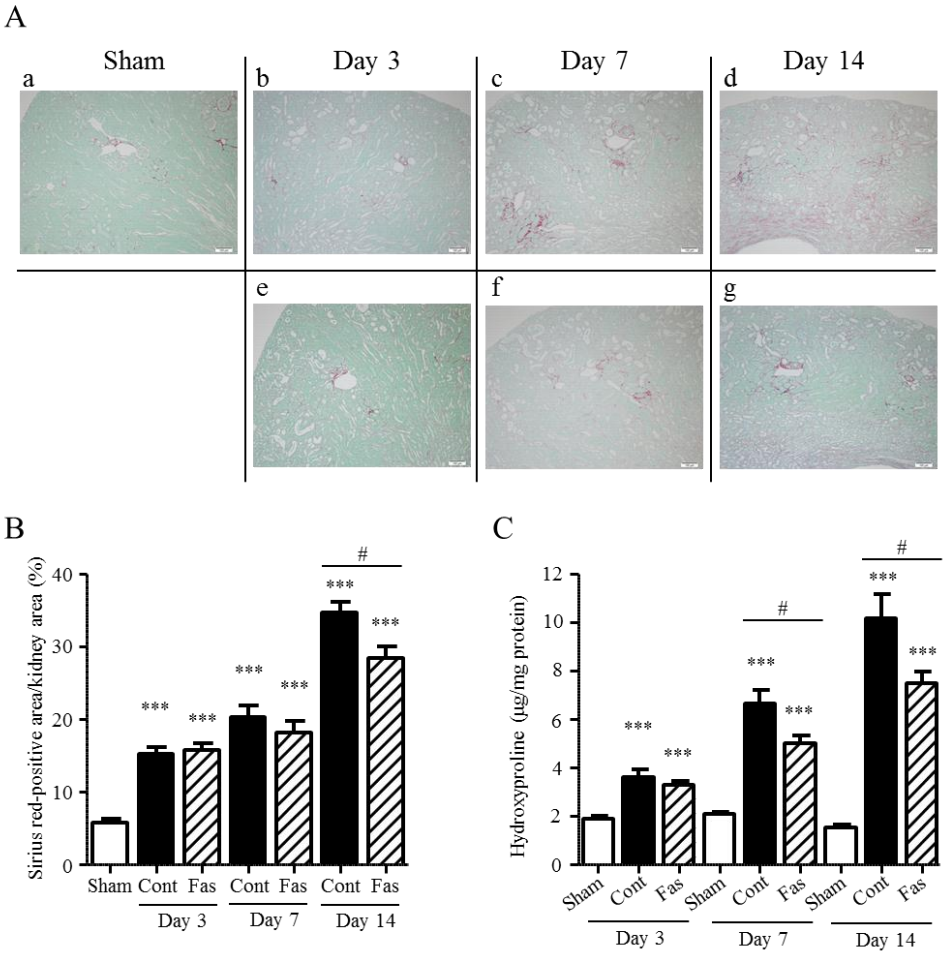

Fig. 10. Sirius Red staining and hydroxyproline content in the kidney

(A) The Sirius Red-stained sections of the sham- and UUO-operated kidneys. Sham (a), UUO-control (b-d), UUO-fasudil (e-g) at days 3, 7, and 14 after UUO, respectively (original magnification x10, scale bars: 100 μm). (B) The Sirius Red-positive area as percentage of total kidney area. (C) The hydroxyproline content in the sham- and UUO-operated kidneys. The symbols are: Sham (open bar); UUO-control (Cont, solid bar); UUO-fasudil (Fas, hatched bar). Results are expressed as mean ± SEM (n= 5-7). *** $P < 0.001$ compared to sham group, # $P < 0.05$ compared to UUO-control mice at the same time point.

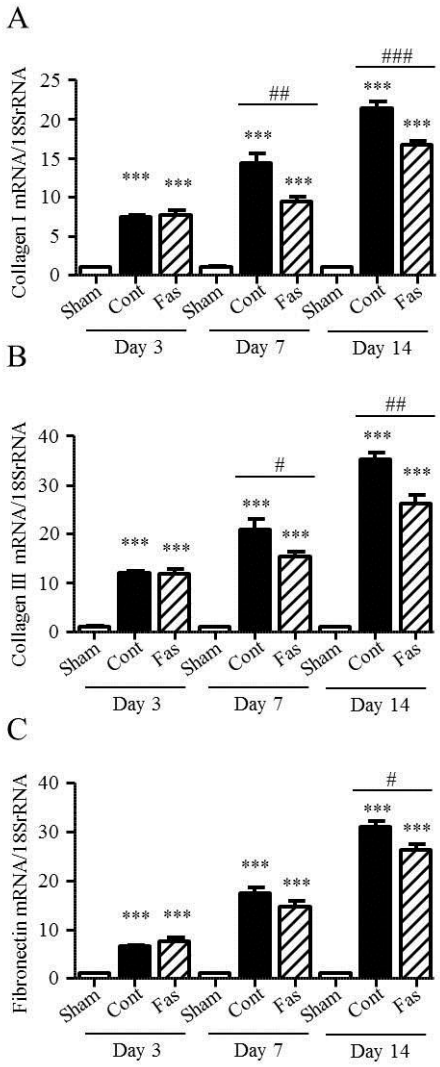

Fig. 11. The mRNA expression of collagen I, III, and fibronectin in the kidney

The mRNA expression of collagen I (A), collagen III (B), and fibronectin (C) in the sham- and UUO-operated kidneys were showed at days 3, 7, and 14 after UUO. The symbols are: Sham (open bar); UUO-control (Cont, solid bar); UUO-fasudil (Fas, hatched bar). Results are expressed as mean ± SEM (n= 6-7). *** $P < 0.001$ compared to sham group, # $P < 0.05$, ## $P < 0.01$, ### $P < 0.001$ compared to UUO-control mice at the same time point.

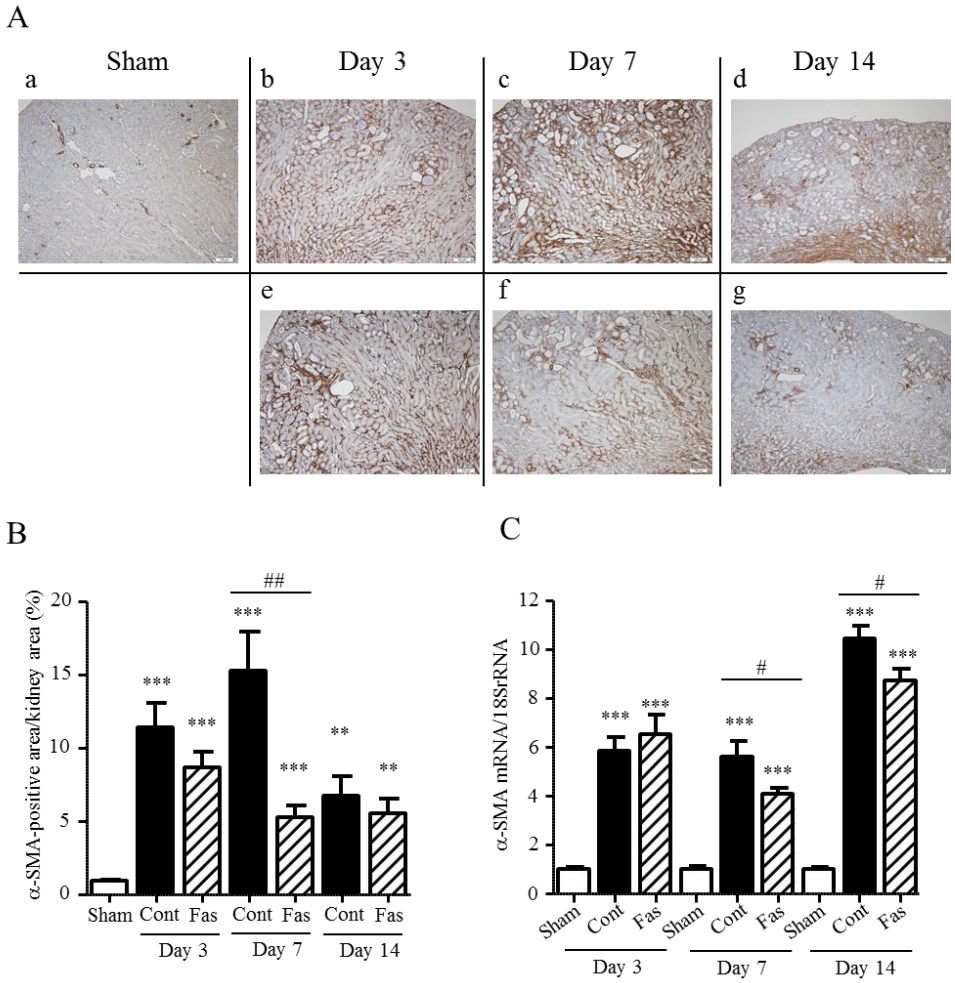

Fig. 12. The expression of α-SMA in the kidney

(A) The α-SMA immunohistochemistry of the sham- and UUO-operated kidneys. Sham (a), UUO-control (b-d), UUO-fasudil (e-g) at days 3, 7, and 14 after UUO, respectively (original magnification x10, scale bars: 100 μm). (B) The α-SMA-positive area as percentage of total kidney area. (C) The mRNA expression of α-SMA was showed at days 3, 7, and 14 after UUO. The symbols are: Sham (open bar); UUO-control (Cont, solid bar); UUO-fasudil (Fas, hatches bar). Results are expressed as mean ± SEM (n= 5-7). ** $P < 0.01$, *** $P < 0.001$ compared to sham group, # $P < 0.05$, ## $P < 0.01$ compared to UUO-control mice at the same time point.

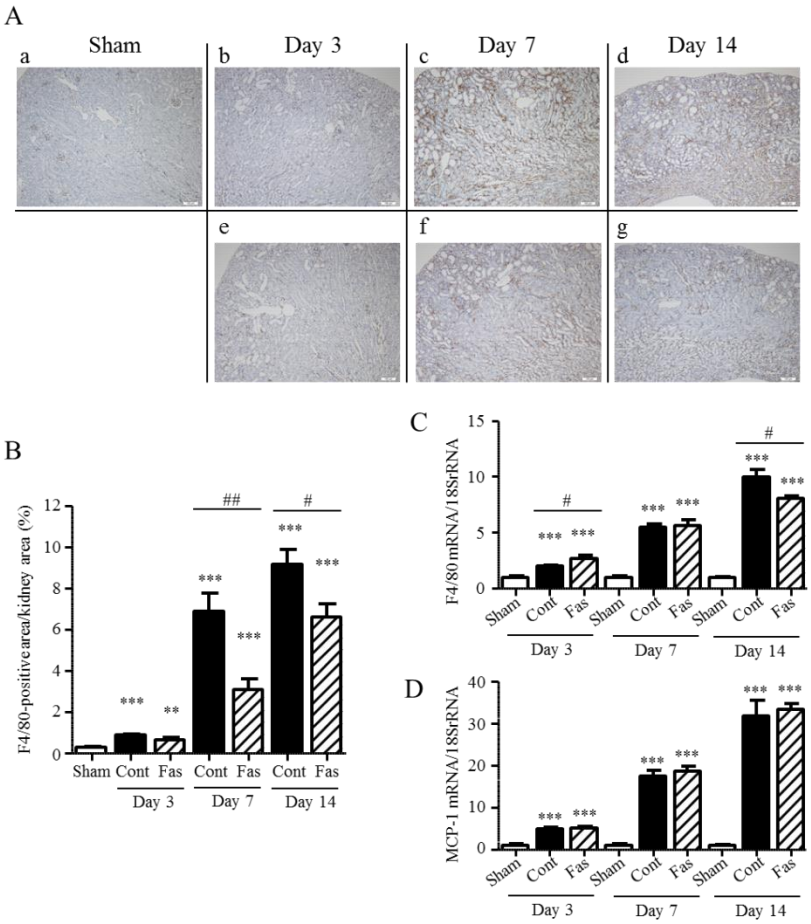

Fig. 13. The expression of F4/80 and MCP-1 in the kidney

(A) The F4/80 immunohistochemistry of the sham- and UUO-operated kidneys. Sham (a), UUO-control (b-d), UUO-fasudil (e-g) at days 3, 7, and 14 after UUO, respectively (original magnification x10, scale bars: 100 μm). (B) The F4/80-positive area as percentage of total kidney area. The mRNA expressions of F4/80 (C) and MCP-1 (D) in the sham- and UUO-operated kidneys were showed at days 3, 7, and 14 after UUO. The symbols are: Sham (open bar); UUO-control (Cont, solid bar); UUO-fasudil (Fas, hatched bar). Results are expressed as mean ± SEM (n= 5-7). ** $P < 0.01$, *** $P < 0.001$ compared to sham group, # $P < 0.05$, ## $P < 0.01$ compared to UUO-control mice at the same time point.

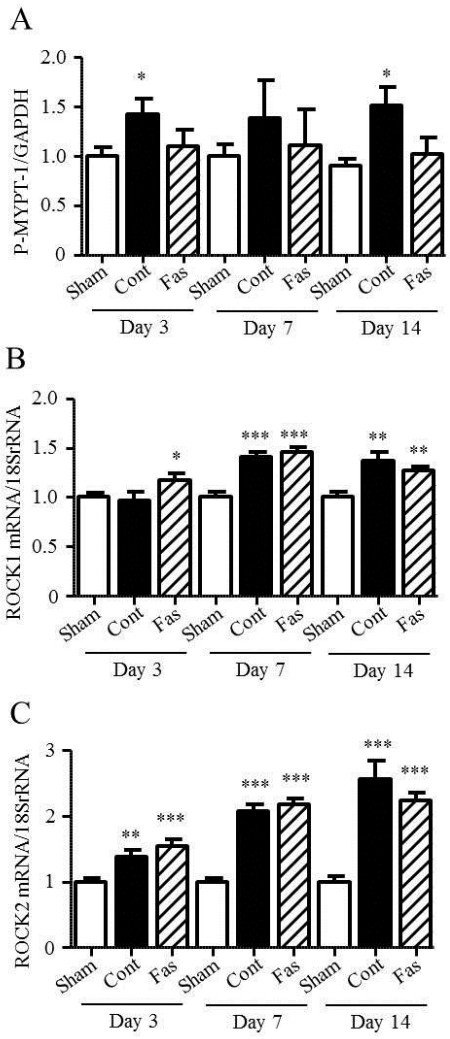

Fig. 14. ROCK activity and the mRNA expression of ROCK1 and ROCK2 in the kidney

(A) Quantitative analysis was showed the relative abundant of the phospho-MYPT-1/GAPDH protein levels ratio detected by the western blotting. The mRNA expressions of ROCK1 (B) and ROCK2 (C) in the sham- and UUO-operated kidneys were showed at days 3, 7, and 14 after UUO. The symbols are: Sham (open bar); UUO-control (Cont, solid bar); UUO-fasudil (Fas, hatched bar). Results are expressed as mean ± SEM (n= 6-7). * $P < 0.05$, ** $P < 0.01$, *** $P < 0.001$ compared to sham group.

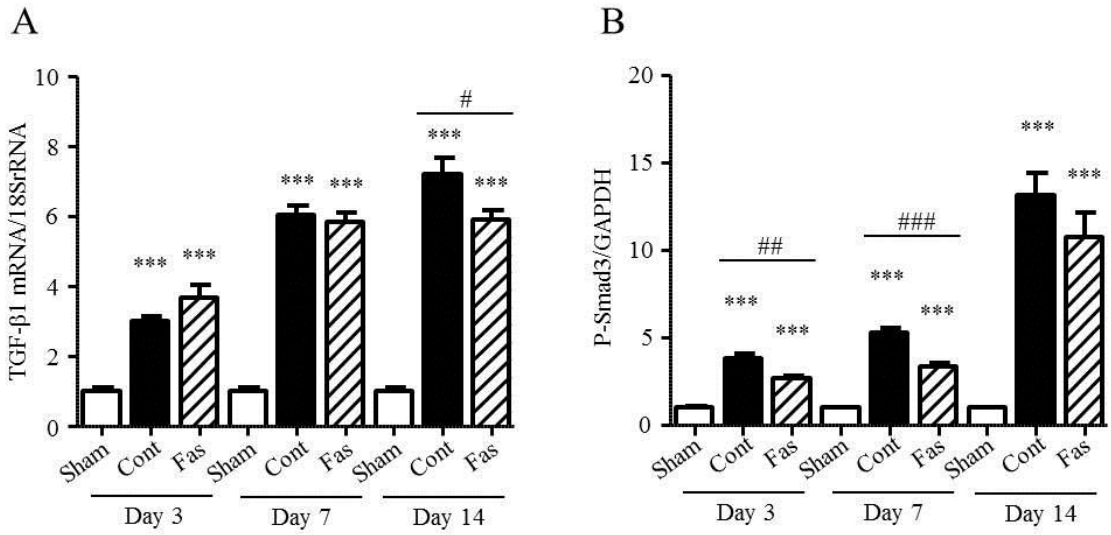

Fig. 15. The expression of TGF-β1 and phospho-Smad3 in the kidney

(A) The mRNA expression of TGF-β1 was showed at days 3, 7, and 14 after UUO. (B) Quantitative analysis was showed the relative abundant of the phospho-Smad3/GAPDH protein levels ratio detected by the western blotting. The symbols are: Sham (open bar); UUO-control (Cont, solid bar); UUO-fasudil (Fas, hatched bar). Results are expressed as mean ± SEM (n= 6-7). *** $P < 0.001$ compared to sham group, # $P < 0.05$, ## $P < 0.01$, ### $P < 0.001$ compared to UUO-control mice at the same time point.

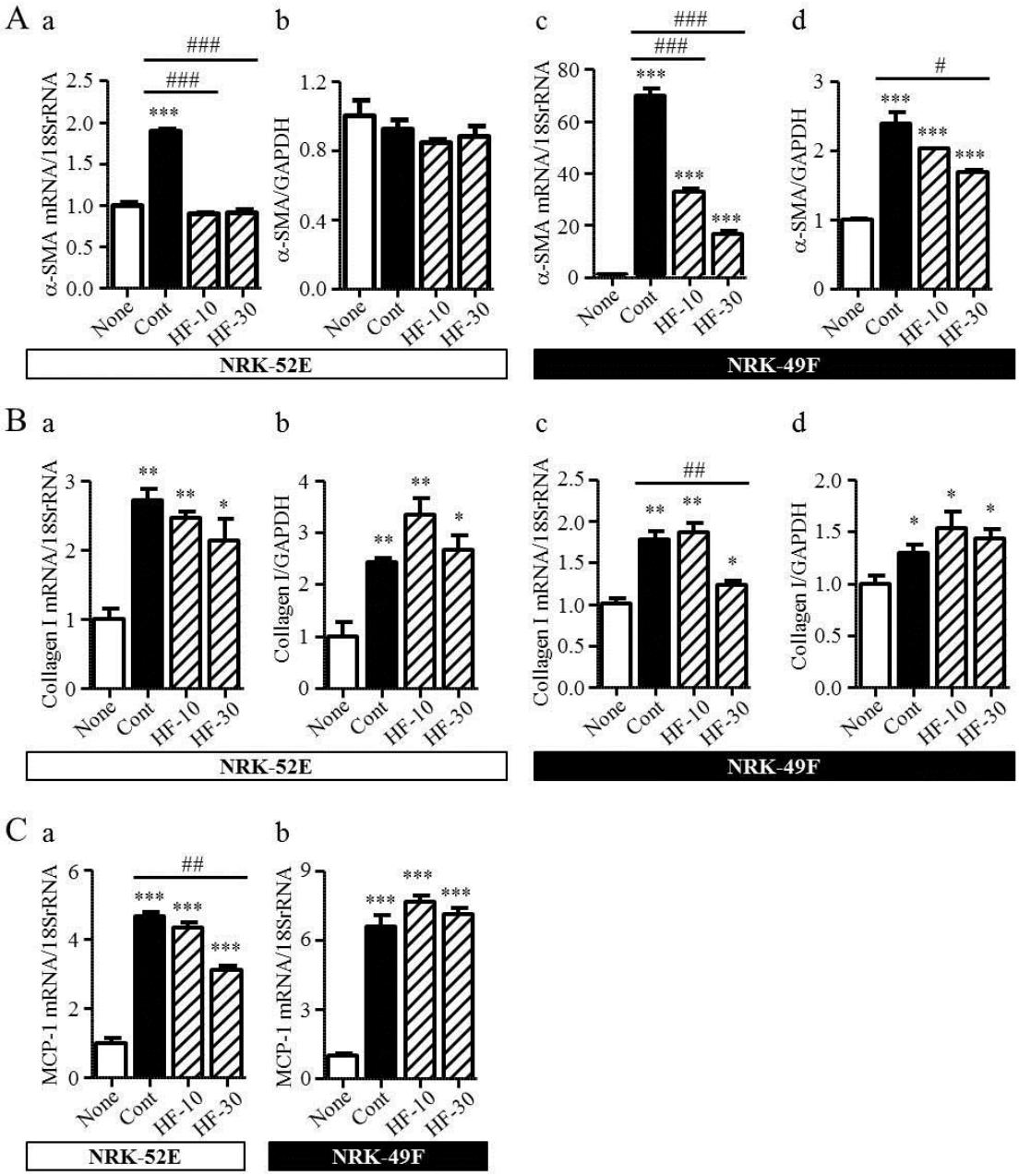

Fig. 16. The expression of α-SMA, collagen I, and MCP-1 in NRK-52E and NRK-49F cells

(A) The α-SMA expression of mRNA and protein were shown in NRK-52E (a, b) and NRK-49F (c, d). (B) The collagen I expression of mRNA and protein were shown in NRK-52E (a, b) and NRK-49F (c, d).

(C) The mRNA expression of MCP-1 was shown in NRK-52E (a) and NRK-49F (b). The symbols are: non-stimulation (None, open bar), TGF-β1 stimulation (Cont, solid bar), pretreatment with 10 or 30μmol/l of hydroxyfasudil before TGF-β1 stimulation (HF-10 or HF-30, hatched bar). Results are expressed as mean ± SEM (n= 3). * $P < 0.05$, ** $P < 0.01$, *** $P < 0.001$ compared to none, # $P < 0.05$, ## $P < 0.01$, ### $P < 0.001$ compared to cont.

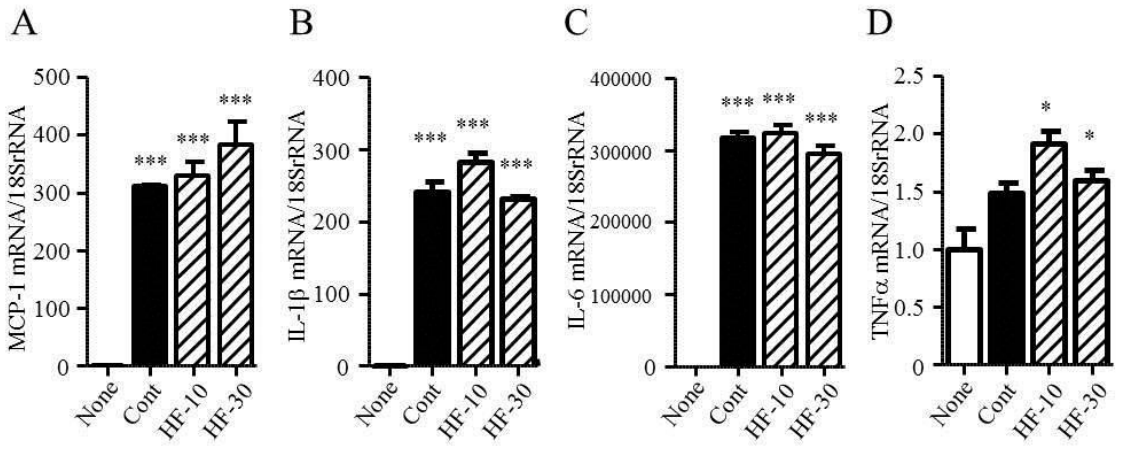

Fig. 17. The mRNA expression of chemokine/cytokines in RAW264.7 cell

The mRNA expressions of MCP-1 (A), IL-1β (B), IL-6 (C), and TNFα (D) were showed in RAW264.7 cell. The symbols are: non-stimulation (None, open bar), LPS stimulation (Cont, solid bar), pretreatment with 10 or 30μmol/l of hydroxyfasudil before LPS stimulation (HF-10 or HF-30, hatched bar). Results are expressed as mean ± SEM (n= 3). * $P < 0.05$, *** $P < 0.001$ compared to none.

Chapter IV

Concluding Remarks

These findings indicate that ROCK clearly affects the progression of renal interstitial fibrosis, suggesting that ROCK exacerbates renal disease as a critical effector molecule.

In the process of the progression of renal injury, several factors increase and stimulate their mutual signaling pathway such as growth factors, cytokines, and chemokines. These factors influence the phase 1 (Fig. 1 and Fig. 18) in the acute state of injury but in chronic state, these as exacerbation factors increase at all times. Given results of the present study, ROCK is particularly involved in the phase 1 (as shown the yellow parts in Fig. 18), cell activation and injury phase. Therefore, a pharmacological inhibition of ROCK affects the progress the whole phases such as EMT, myofibroblast activation, proliferation, macrophage infiltration, inflammation, and ECM production.

Moreover, other pathways were affected by fasudil, a ROCK inhibitor in mice UUO model. Also, many inflammatory-related genes totally elevated after the onset of UUO. Fasudil reduced the deteriorating expression of these genes. Thus, the pharmacological inhibition of ROCK comprehensively inhibits fibrogenic signaling pathways, monocyte/macrophage infiltration, and activation of the inflammatory responses in the renal interstitium.

In conclusion, ROCK inhibitor has the multimodal effects on renal

interstitial fibrosis and would be a promising choice for the treatment of renal diseases.

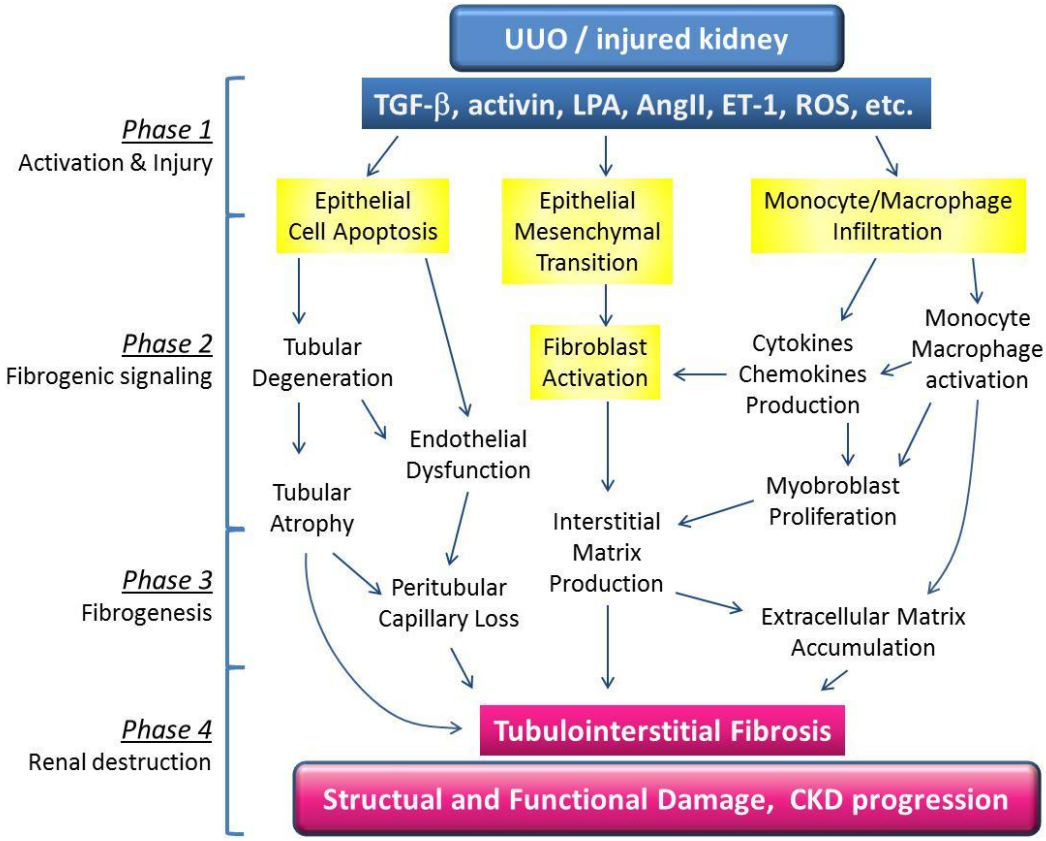

Fig. 18. Scheme of renal interstitial fibrosis and target points of ROCK inhibitors

Chapter V

Acknowledgment

I wish to express sincere appreciation to the many individuals who have offered support, inspiration, and encouragement throughout this study.

I would like to express my special gratitude to Prof. Dr. Akiyoshi Fukamizu who provided me this opportunity, constant guidance, supports, and encouragement.

I would like to express my sincere appreciation to Dr. Junji Ishida for his guidance and generous supports.

I would like to express my sincere appreciation to Prof. Dr. Shuh Narumiya, Director of Medical Innovation Center, Graduate School of Medicine, Kyoto University, who kindly permit to use the ROCK2 HKO mice. I would like to express my deepest appreciation to Dr. Yasuhiro Egi who supports, operates for the UUO model together and provide me valuable suggestions, comments, and encouragement. I would like to express my sincere appreciation to Dr. Tetsuhiro Kakimoto and Dr. Hiroyuki Utsumi who examine and analyze the histological studies.

I would like to express my sincere appreciation to Dr. Kenji Arakawa, Dr. Rikako Yamauchi, and Dr. Taku Sato who provide me this opportunity and support this study. Finally I would like to express my sincere appreciation to Dr. Kazuo Suzuki, General Manager of Department II, Pharmacology Research Laboratories II, Mitsubishi Tanabe Pharma Corporation, for his supports.

Itsuko Baba

Chapter VI

References

1. Genovese F, Manresa AA, Leeming DJ, Karsdal MA and Boor P: The extracellular matrix in the kidney: a source of novel non-invasive biomarkers of kidney fibrosis? Fibrogenesis & Tissue Repair 7: 4-17, 2014.
2. Lopez-Novoa JM, Martinez-Salgado C, Rodriguez-Pena AB and Hernandez FJL: Common pathophysiological mechanisms of chronic kidney disease: Therapeutic perspectives. Pharmacol Ther 128: 61-81, 2010.
3. Klein J, Kavvadas P, Prakoura N, Karagianni F, Schanstra JP, Bascands JL and Charonis A: Renal fibrosis: Insight from proteomics in animal models and human disease. Proteomics 11: 805-815, 2011.
4. Chevalier RL, Forbes MS and Thornhill BA: Ureteral obstruction as a model of renal interstitial fibrosis and obstructive nephropathy. Kidney Int 75: 1145-1152, 2009.
5. Chevalier RL: Obstructive nephropathy: towards biomarker discovery and gene therapy. Nat Clin Pract Nephrol 2: 157-168, 2006.
6. Truong LD, Gaber L and Eknoyan G: Obstructive Uropathy. Contrib Nephrol Basel Karger 169: 311-326, 2011.
7. Yang HC, Zuo Y and Fogo AB: Models of chronic kidney disease. Drug Discov Today Dis Models 7: 13-19, 2010.
8. Satoh K, Fukumoto Y and Shimokawa H: Rho-kinase: important new therapeutic target in cardio- vascular diseases. Am J Physiol Heart Circ Physiol 301: H287-H296, 2011.
9. Hahmann C and Schroeter T: Rho-kinase inhibitors as therapeutics: from pan inhibition to isoform selectivity. Cell Mol Life Sci 67: 171-177, 2010.
10. Olson MF: Applications for ROCK kinase inhibition. Curr Opin Cell

Biol 20: 242-248, 2008.
11. Amin E, Dubey BN, Zhang SC, Gremer L, Dvorsky R, Moll JM, Taha MS, Nagel-Steger L, Piekorz RP, Somlyo AV and Ahmadian MR: Rho-kinase: regulation, (dys)function, and inhibition. Biol Chem 394: 1399-1410, 2013.
12. Schofield AV and Bernard O: Rho-associated coiled-coil kinase (ROCK) signaling and disease. Crit Rev Biochem Mol Biol 48: 301-316, 2013.
13. Shi J and Wei L: Rho kinase in the regulation of cell death and survival. Arch Immunol Ther Exp 55: 61-75, 2007.
14. Ming D, Yan BP, Liao JK, Lam YY, Yip GWK and Yu CM: Rho-kinase inhibition: a novel therapeutic target for the treatment of cardiovascular diseases. Drug Discov Today 15: 622-629, 2010.
15. Budzyn K, Marley PD and Sobey CG: Targeting Rho and Rho-kinase in the treatment of cardiovascular disease. Trends Pharmacol Sci 27: 97-104, 2006.
16. Shimokawa H and Rashid M: Development of Rho-kinase inhibitors for cardiovascular medicine. Trends Pharmacol Sci 28: 296-302, 2007.
17. Kushiyama T, Oda T, Yamamoto K, Higashi K, Watanabe A, Takechi H, Uchida T, Oshima N, Sakurai Y, Miura S and Kumagai H: Protective effects of Rho kinase inhibitor fasudil on rats with chronic kidney disease. Am J Physiol Renal Physiol 304: F1325-F1334, 2013.
18. Nishikimi T, Koshikawa S, Ishikawa Y, Akimoto K, Inaba C, Ishimura K, Ono H and Matsuoka H: Inhibition of Rho-kinase attenuates nephrosclerosis and improves survival in salt-loaded spontaneously hypertensive stroke-prone rats. J Hypertens 25: 1053-1063, 2007.
19. Kanda T, Wakino S, Hayashi K, Homma K, Ozawa Y and Saruta T: Effect of fasudil on Rho-kinase and nephropathy in subtotally nephrectomized spontaneously hypertensive rats. Kidney Int 64: 2009-2019, 2003.
20. Xie X, Peng J, Chang X, Huang K, Huang J, Wang S, Shen X, Liu P

and Huang H: Activation of RhoA/ROCK regulates NF-kappaB signaling pathway in experimental diabetic nephropathy. Mol Cell Endocrinol 369: 86-97, 2013.
21. Zhou H, Li YJ, Wang M, Zhang LH, Guo BY, Zhao ZS, Meng FL, Deng YG and Wang RY: Involvement of RhoA/ROCK in myocardial fibrosis in a rat model of type 2 diabetes. Acta Pharmacol Sin 32: 999-1008, 2011.
22. Pan P, Shen M, Yu H, Li Y, Li D and Hou T: Advances in the development of Rho-associated protein kinase (ROCK) inhibitors. Drug Discov Today 18: 1323-1333, 2013.
23. Loirand G, Guerin P and Pacaud P: Rho kinases in cardiovascular physiology and pathophysiology. Circ Res 98: 322-334, 2006.
24. Muller BK, Mack H and Teusch N: Rho kinase, a promising drug target for neurological disorders. Nat Rev Drug Discov 4: 387-398, 2005.
25. Morgan-Fisher M, Wewer UM and Yoneda A: Regulation of ROCK activity in cancer. J Histochem Cytochem 61: 185-198, 2012.
26. Shimokawa H and Takeshita A: Rho-kinase is an important therapeutic target in cardiovascular medicine. Arterioscler Thromb Vasc Biol 25: 1767-1775, 2005.
27. Nagatoya K, Moriyama T, Kawada N, Takeji M, Oseto S, Murozono T, Ando A, Imai E and Hori M: Y-27632 prevents tubulointerstitial fibrosis in mouse kidneys with unilateral ureteral obstruction. Kidney Int 61: 1684-1695, 2002.
28. Satoh S, Yamaguchi T, Hitomi A, Sato N, Shiraiwa K, Ikegaki I, Asano T and Shimokawa H: Fasudil attenuates interstitial fibrosis in rat kidneys with unilateral ureteral obstruction. Eur J Pharmacol 455: 169-174, 2002.
29. Takeda Y, Nishikimi T, Akimono K, Matsuoka H and Ishimitsu T: Benefical effects of a combination of Rho-kinase inhibitor and ACE inhibitor on tubulointerstitial fibrosis induced by unilateral ureteral obstruction. Hypertens Res 33: 965-973, 2010.

30. Fu P, Liu F, Su S, Wang W, Huang XR, Entman ML, Schwartz RJ, Wei L and Lan HY: Signaling mechanism of renal fibrosis in unilateral ureteral obstructive kidney disease in ROCK1 knockout mice. J Am Soc Nephrol 17: 3105-3114, 2006.
31. Rikitake Y, Oyama N, Wang CY, Noma K, Satoh M, Kim HH and Liao JK: Decreased perivascular fibrosis but not cardiac hypertrophy in ROCK1+/- haploinsufficient mice. Circulation 112: 2959-2965, 2005.
32. Li Q, Xu Y, Li X, Guo Y and Liu G: Inhibition of Rho-kinase ameliorates myocardial remodeling and fibrosis in pressure overload and myocardial infarction: role of TGF-beta1-TAK1. Toxicol Lett 211: 91-97, 2012.
33. Sun GP, Kohno M, Guo P, Nagai Y, Miyata K, Fan YY, Kimura S, Kiyomoto H, Ohmori K, Li DT, Abe Y and Nishiyama A: Involvements of Rho-kinase and TGF-beta pathways in aldosterone-induced renal injury. J Am Soc Nephrol 17: 2193-2201, 2006.
34. Zhang YM, Bo J, Taffet GE, Chang J, Shi J, Reddy AK, Michael LH, Schneider MD, Entman ML, Schwartz RJ and Wei L: Targeted deletion of ROCK1 protects the heart against pressure overload by inhibiting reactive fibrosis. FASEB J 20: 916-925, 2006.
35. Zhou L, Liu F, Huang XR, Chen H, Chung AC, Shi J, Wei L, Lan HY and Fu P: Amelioration of albuminuria in ROCK1 knockout mice with streptozotocin-induced diabetic kidney disease. Am J Nephrol 34: 468-475, 2011.
36. Okamoto R, Li Y, Noma K, Hiroi Y, Liu PY, Taniguchi M, Ito M and Liao JK: FHL2 prevents cardiac hypertrophy in mice with cardiac-specific deletion of ROCK2. FASEB J 27: 1439-1449, 2013.
37. Thumkeo D, Keel J, Ishizaki T, Hirose M, Nonomura K, Oshima H, Oshima M, Taketo MM and Narumiya S: Targeted disruption of the mouse Rho-associated kinase 2 gene results in intrauterine growth retardation and fetal death. Mol Cell Biol 23: 5043-5055, 2003.

38. Woessner JF: The determination of hydroxyproline in tissue and protein samples containing small proportions of this imino acid. Arch Biochem Biophys 93: 440-447, 1961.
39. Kari IK, Ossi L and Darwin JP: Modifications of a specific assay for hydroxyproline in urine. Anal Biochem 19: 249-255, 1967.
40. Liu Y: Epithelial to mesenchymal transition in renal fibrogenesis: pathologic significance, molecular mechanism, and therapeutic intervention. J Am Soc Nephrol 15: 1-12, 2004.
41. Patel S, Takagi KI, Suzuki J, Imaizumi A, Kimura T, Mason RM, Kamimura T and Zhang Z: RhoGTPase activation is a key step in renal epithelial mesenchymal transdifferentiation. J Am Soc Nephrol 16: 1977-1984, 2005.
42. Rodrigues DR, Carvajal GG, Sánchez LE, Rodríguez VJ, Rodrigues DR, Selgas R, Ortiz A, Egido J, Mezzano S and Ruiz OM: Pharmacological modulation of epithelial mesenchymal transition caused by angiotensin II. Role of ROCK and MAPK pathways. Pharm Res 25: 2447-2461, 2008.
43. Li Y, Zhu W, Tao J, Xin P, Liu M, Li J and Wei M: Fasudil protect the heart against ischemia-reperfusion injury by attenuating endoplasmic reticulum stress and modulating SERCA activity: The differential role for PI3K/Akt and JAK2/STAT3 signaling pathways. PLoS ONE 7: e48115-48126, 2012.
44. Kentrup D, Reuter S and Schnockel U, Grabner A, Edemir B, Pavenstadt H, Schober O, Schafers M, Schlatter E and Bussemaker E: Hydroxyfasudil-mediated inhibition of ROCK1 and ROCK2 improves kidney function in rat renal acute ischemia-reperfusion injury. PLoS ONE 6: e26419-e26431, 2011.
45. Matoba K, Kawanami D and Okada R, Tsukamoto M, Kinoshita J, Ito T, Ishizawa S, Kanazawa Y, Yokota T, Murai N, Matsufuji S, Takahashi-Fujigasaki J and Utsunomiya K: Rho-kinase inhibition privents the progression of diabetic nephropathy by downregulating

hypoxia-inducible factor 1α. Kidney Int 84: 545-554, 2013.
46. Diah S, Zhang GX, Nagai Y, Zhang W, Gang L, Kimura S, Hamid MRWA, Tamiya T, Nishiyama A and Hitomi H: Aldosterone induced mypfibroblastic transdifferentiation and collagen gene expression through the Rho-kinase dependent signaling pathway in rat mesangial cells. Exp Cell Res 314: 3654-3662, 2008.
47. Wei J, Li Z, Ma C, Zhan F, Wu W, Han H, Huang Y, Li W, Chen D and Peng Y: Rho kinase pathway is likely responsible for the profibrotic actions of aldosterone in renal epithelial cells via inducing epithelial-mesenchymal transition and extracellular matrix excretion. Cell Biol Int 37: 725-730, 2013.
48. Manickam N, Patel M, Griendling KK, Gorin Y and Barnes JL: RhoA/Rho kinase mediates TGF-β1-induced kidney myofibroblast activation through Poldip2/Nox4-derived reactive oxygen species. Am J Physiol Renal Physiol 307: F159-F171, 2014.
49. Kakimoto T, Kimata H, Iwasaki S, Fukunari A and Utsumi H: Automated recognition and quantification of pancreatic islets in Zucker diabetic fatty rats treated with exendin-4. J Endocrinol 216: 13-20, 2013.
50. Shen B, Liu X, Fan Y and Qiu J: Macrophages regulate renal fibrosis through modulating TGFβ superfamily signaling. Inflammation 15: published online, 2014.
51. Eddy AA, Lopez-Guisa JM, Okamura DM and Yamaguchi I: Investigating mechanizes of chronic kidney disease in mouse models. Pediatr Nephrol 27: 1233-1247, 2012.
52. Ballhause TM, Soldati R and Mertens PR: Sources of myofibroblats in kidney fibrosis: All answers are correct, however to different extent! Int Urol Nephrol 46: 659-664, 2014.
53. Duffield JS: Cellular and molecular mechanisms in kidney fibrosis. J Clin Invest 124: 2299-2306, 2014.
54. Pan SY, Chang YT and Lin SL: Microvascular pericytes in healthy and

diseased kidneys. Int J Nephrol Renovascul Disease 7: 39-48, 2014.
55. LeBleu VS, Taduri G, O'Connell J, Teng Y, Cooke VG, Wada C, Sugimoto H and Kalluri R: Origin and function of myofibroblasts in kidney fibrosis. Nat Med 19: 1047-1054, 2013.
56. Jang HS, Kim JI, Jung KJ, Kim J, Han KH and Park KM: Bone marrow-derived cells play a major role in kidney fibrosis via proliferation and differentiation in the infiltrated site. Biochim Biophys Acta 1832: 817-825, 2013.
57. Qin J, Xie YY, Huang L, Yuan QJ, Mei WJ, Yuan XN, Hu GY, Cheng GJ, Tao LJ and Peng ZZ: Fluorofenidone inhibits nicotinamide adeninedinucleotide phosphate oxidase via PI3K/Akt pathway in the pathogenesis of renal interstitial fibrosis. Nephrology 18: 690-699, 2013.
58. Gu L, Gao Q, Ni L, Wang M and Shen F: Fasudil inhibits epithelial-myofibroblast transdifferentiation of human renal tubular epithelial HK-2 cells induced by high glucose. Chem Pharm Bull 61: 688-694, 2013.
59. Gande MT, Perez-Barriocanal F and Lopez-Novoa JM: Role of inflammation in tubule-interstitial damage associated to obstructive nephropathy. J Inflamm 7: 19-32, 2010.
60. Wang Y and Harris DCH: Macrophages in renal disease. J Am Soc Nephrol 22: 21-27, 2011.
61. Chung ACK and Lan HY: Chemokines in renal injury. J Am Soc Nephrol 22: 802-809, 2011.
62. Liu N, Tolbert E, Pang M, Ponnusamy MI, Yan H and Zhuang S: Suramin inhibits renal fibrosis in chronic kidney disease. J Am Soc Nephrol 22: 1064-1075, 2011.
63. Pang M, Ma Li, Gong R, Tolbert E, Mao H, Ponnusamy M, Chin YE, Yan H, Dworkin LD and Zhuang S: A novel STAT3 inhibitor, S31-201, attenuates renal interstitial fibroblast activation and interstitial fibrosis in obstructive nephropathy. Kidney Int 78: 257-268, 2010.

64. Meng XM, Huang XR and Xiao J: Diverse roles of TGF-β receptor II in renal fibrosis and inflammation *in vivo* and *in vitro*. J Pathol 227: 175-188, 2012.
65. Anders HJ and Ryu M: Renal microenviroments and macrophage phenotypes determine progression or resolution of renal inflammation and fibrosis. Kidney Int 80: 915-925, 2011.
66. Ricardo SD, Goor HV and Eddy AA: Macrophage diversity in renal injury and repair. J Clin Invest 118: 3522-3530, 2008.